Article

Current Biology

The biology and chemistry of a mutualism between a soil bacterium and a mycorrhizal fungus

Graphical abstract

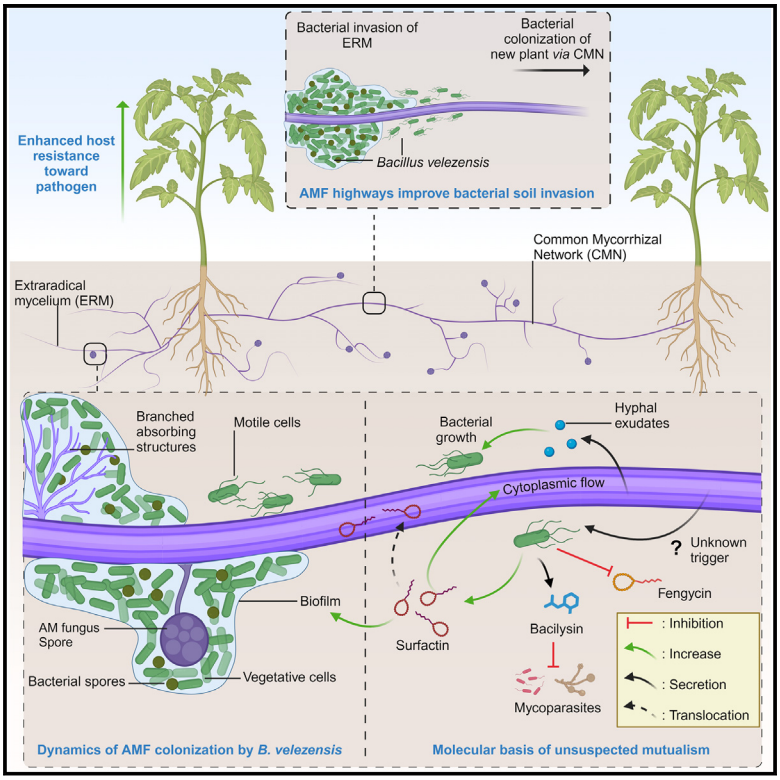

Highlights

- *B. velezensis* colonizes the entire mycelial network more efficiently than roots
- *Bacillus* uses fungal hyphae as highways for soil invasion and to colonize new plant
- The lipopeptide surfactin plays key roles in the chemical ecology of the interaction
- The microbial partnership enhances the systemic resistance of tomato against *Botrytis*

Authors

Adrien Anckaert, Stéphane Declerck, Laure-Anne Poussart, ..., Anthony Argüelles-Arias, Maryline Calonne-Salmon, Marc Ongena

Correspondence

adrien.anckaert@uliege.be (A.A.), marc.ongena@uliege.be (M.O.)

In brief

Anckaert et al. investigate the dynamics of *Rhizophagus* hyphae colonization by *B. velezensis*. Reduced production of bacterial toxic metabolites triggered by the fungus leads to an unsuspected stable coexistence. This interaction brings benefits to both microbes and provides positive effects to the host plant, which is more resistant to disease.

Anckaert et al., 2024, Current Biology *34*, 4934–4950
November 4, 2024
https://doi.org/10.1016/j.cub.2024.09.019

CellPress

CellPress
OPEN ACCESS

Current Biology

Article

The biology and chemistry of a mutualism between a soil bacterium and a mycorrhizal fungus

Adrien Anckaert,[1,3,*] Stéphane Declerck,[2,3] Laure-Anne Poussart,[1] Stéphanie Lambert,[1] Catherine Helmus,[1] Farah Boubsi,[1] Sébastien Steels,[1] Anthony Argüelles-Arias,[1] Maryline Calonne-Salmon,[2] and Marc Ongena[1,4,5,*]

[1]Microbial Processes and Interactions Laboratory, TERRA Teaching and Research Center, University of Liège - Gembloux Agro-Bio Tech, Avenue de la Faculté d'Agronomie, Bat. 9B, 5030 Gembloux, Belgique

[2]Laboratory of Mycology, Earth and Life Institute, Université catholique de Louvain-UCLouvain, Croix du Sud 2, L7.05.06, 1348 Louvain-la-Neuve, Belgique

[3]These authors contributed equally

[4]X (formerly Twitter): microbeinteract

[5]Lead contact

*Correspondence: adrien.anckaert@uliege.be (A.A.), marc.ongena@uliege.be (M.O.)

https://doi.org/10.1016/j.cub.2024.09.019

SUMMARY

Arbuscular mycorrhizal (AM) fungi (e.g., *Rhizophagus* species) recruit specific bacterial species in their hyphosphere. However, the chemical interplay and the mutual benefit of this intricate partnership have not been investigated yet, especially as it involves bacteria known as strong producers of antifungal compounds such as *Bacillus velezensis*. Here, we show that the soil-dwelling *B. velezensis* migrates along the hyphal network of the AM fungus *R. irregularis*, forming biofilms and inducing cytoplasmic flow in the AM fungus that contributes to host plant root colonization by the bacterium. During hyphosphere colonization, *R. irregularis* modulates the biosynthesis of specialized metabolites in *B. velezensis* to ensure stable coexistence and as a mechanism to ward off mycoparasitic fungi and bacteria. These mutual benefits are extended into a tripartite context via the provision of enhanced protection to the host plant through the induction of systemic resistance.

INTRODUCTION

Arbuscular mycorrhizal (AM) fungi are keystone beneficial microorganisms within rhizobiomes, forming symbiotic associations with more than two-thirds of terrestrial plants. They improve nutrients uptake (P and N) by plants via their extensive and dense extraradical mycelium (ERM), extending tens of cm away from the roots and exploring soil pores via hyphae with diameters up to 10 times lower than that of root hairs.[1–3] The ERM also enables the interconnection of plants of the same or different species to form common mycorrhizal networks. Plants can receive warning signals via these common mycorrhizal networks in response to pest and pathogen attacks and potentially exchange nutrients.[4–7] Some AM fungal species also have the potential to increase plant systemic resistance against below- and above-ground pathogens via mechanisms resembling induced systemic resistance (ISR).[8–10]

AM fungi exploit between 4% and 20% of the total carbon synthesized by the host plant to feed their own metabolic processes, to ensure growth[11] but also to fuel the catabolism of microbes developing at the hyphal surface in the so-called hyphosphere where carbon-rich fungal exudates are released. As plants do via rhizodeposits, AM fungi thus recruit a wide range of bacterial species, forming hyphosphere-associated microbiomes that start to be quite well characterized phylogenetically.[12–20] A few recent studies have highlighted the benefits brought by bacteria to the fungus by the mineralization of organic P and N sources.[14,19,21,22] Similarly, AM fungal hyphae may serve as conduits for certain phosphate-solubilizing bacteria to reach organic P patches in the soil.[23] However, the molecular basis and phenotypic outcomes of such interkingdom interaction between AM fungi and bacteria dwelling at the hyphal surface are still poorly described.[14,18] How and to what extent such cooperation could be established with biocontrol bacteria known as strong antagonists of fungi remain unexplored, despite the potential benefit of combining these two microorganisms to improve plant protection against pests and diseases.

In this work, we used custom-designed *in vitro*[15,24–26] and *in planta* systems with *Solanum lycopersicum*[16,18,27] and *Solanum tuberosum*[28] to explore the interkingdom interaction between several *Rhizophagus* species well characterized as plant mutualistic AM fungi and *Bacillus velezensis* as model species of rhizobacteria producing bioactive secondary metabolites (BSMs) with antifungal activity. To study the dynamics of bacterial colonization along the AM fungal ERM, we used a tripartite *in vitro* cultivation system offering the advantage of non-destructive time-lapse observations, allowing the monitoring of interactions between both microorganisms in the absence of any other microbial protagonist. Combining molecular and analytical analyses, we identified key BSMs that contribute to the establishment of a compatible interaction and elucidate how the AM fungus (AMF) drives BSM production in the bacterium and its consequence on antifungal activities of *B. velezensis*. Importantly, we demonstrated that the cooperation between the two

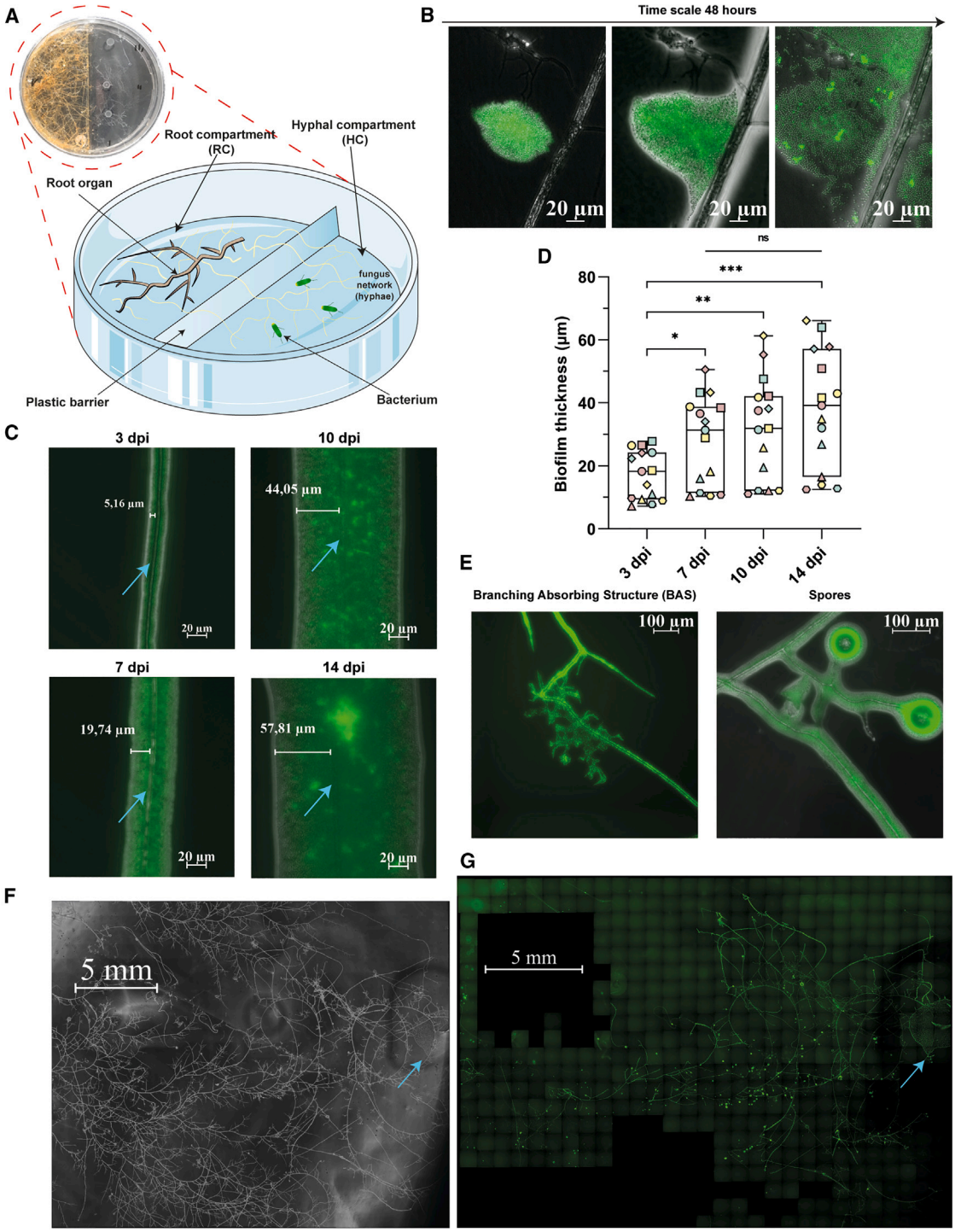

Figure 1. *B. velezensis* behavior and colonization along AM fungal hyphae

(A) Picture (red circle) and schematic view of the *in vitro* bi-compartmented Petri plate system allowing to perform live cell microscopy imaging. The Petri plate was separated in two compartments by a plastic barrier, with a root compartment (RC) containing a Ri transfer DNA (T-DNA) transformed *Daucus carota* root clone DC2 associated to *Rhizophagus irregularis* and a hyphal compartment (HC) containing only hyphae of *R. irregularis*. In the HC, the hyphae were allowed to proliferate on solid MSR medium without any added carbon source and solidified with agarose (MSR^{min}). Once the hyphae were well established in the HC, *Bacillus velezensis* was inoculated on the hyphae to study their interaction. This system offers the advantage of non-destructive time-lapse observations without confounding effects with unwanted microbial contaminants. Brown, transformed root organ of *D. carota*; white, hyphae of *R. irregularis*; green, cells of *B. velezensis*.

(B) Microscopic picture of *B. velezensis* GA1 labeled with GFP, attracted and established on the hyphae of *R. irregularis* by chemotaxis (timescale of 48 h).

(legend continued on next page)

microorganisms confers increased protection of tomatoes against *Botrytis cinerea*.

RESULTS

B. velezensis efficiently colonizes the hyphae of *R. irregularis* and expands rapidly along the ERM network

We first studied the spatiotemporal dynamics of the physical interaction between *B. velezensis* and *R. irregularis* in the hyphal zone of bi-compartmented plates as illustrated in Figure 1A. The *B. velezensis* strain GA1 was selected for its recognized biocontrol potential and its fully characterized genome and secondary metabolome.[29–32] The *R. irregularis* strain MUCL 41833 was selected for its use in the understanding of AM fungal interaction with rhizobacteria[21,33] and its well-known beneficial effects on plant growth and resistance against biotic stresses.[34,35]

We used mature systems with well-developed ERM network obtained approximately 3 months after initial mycorrhization of roots. Time-lapse microscopy imaging revealed that GFP-tagged *B. velezensis* cells inoculated at short distance (~20 μm) from the hyphae of *R. irregularis* moved to and established on the hyphal surface within 48 h (Figure 1B), suggesting a behavior similar to the chemotaxis observed with plant roots.[36,37] Then, the bacteria spread over the *R. irregularis* mycelium as motile cells but rapidly switch within hours to a sessile state, allowing the establishment of multicellular colonies (Videos S1 and S2). This leads to the development of a homogeneous bacterial cell layer along the hyphae as illustrated by the significant increase in colony thickness within the first days post inoculation (dpi) of the bacterium on short segments (Figures 1C and 1D) of runner hyphae. This biofilm-like layer rapidly expanded along the runner hyphae and colonized other structures of the ERM such as spores and branched absorbing structures specialized in nutrient uptake (Figures 1E and S1A).[38] As compared with the wild type, formation of this thick layer and hyphae colonization were significantly reduced upon testing the mutants *ΔepsA-O* and *ΔtasA* repressed, respectively, in the synthesis of exopolysaccharides or TasA protein representing essential components of the biofilm matrix in *Bacillus* (Figure S2).[36,39] This indicated that the observed bacterial cell layer corresponds to a biofilm stricto sensu.

Further imaging at a larger scale showed that *B. velezensis* spread over the major part of the dense ERM network within 3 days (Figures 1F and 1G). We calculated an average expansion rate for the bacterium (colonization speed) of 5.6 mm/day on the surface of hyphae, which was significantly higher than observed for the colonization of *Daucus carota* hairy roots (1.2 mm/day) (Figures 2A and S1B). It thus revealed a quite fast invasion of distal parts of the ERM by *B. velezensis* (Figure 2B) compared to roots (Figure S1C). In support to imaging, *B. velezensis* colonization density was also quantified by colony-forming units (CFUs) plate counting at 3, 7, and 14 dpi. Data showed 20-fold higher populations at the surface of *R. irregularis* hyphae compared with *D. carota* roots (Figure 2C), further indicating that *B. velezensis* is more prone to colonize *R. irregularis* hyphae than roots in the early stage of interaction. We further tested the ability of *B. velezensis* to colonize other species within the *Rhizophagus* genus. Our results indicated that the bacterium was more prone to colonize the hyphae of *R. irregularis* compared to *R. clarus*, *R. aggregatus*, and *R. intraradices* (Figure S1D). Even considering the lowest colonization rates on *R. aggregatus* and *R. intraradices*, bacterial populations on hyphae (644 ± 176.5 and 240.2 ± 49.95 CFU/mm^2, respectively; mean ± SD) were still at least 2.5 times higher than on roots (53.12 ± 24.98 CFU/mm^2). These results underscore the influence of genetic diversity within the *Rhizophagus* genus on the interaction dynamics with *B. velezensis* and support the general trend of higher bacterial colonization on AM fungal hyphae compared to plant roots. This may be due to the formation of an homogeneous biofilm along hyphae, while colonization of roots is known to occur at preferential zones via the formation of bacterial macrocolonies.[40,41] In addition, we also observed that the relative proportion of spores compared to vegetative cells within the *B. velezensis* population colonizing the hyphae of *R. irregularis* was significantly lower (1.6-fold at 7 dpi) than the one colonizing *D. carota* roots (Figure S1E). This high proportion of metabolically active cells in the AM fungal-associated biofilm may thus also reflect a bacterial community more prompt to colonize the fungal host than plant roots.

We next wanted to monitor *B. velezensis* colonization under more realistic conditions using mycorrhized *S. tuberosum* plants in greenhouse conditions. We used a custom made setup with two pots,[16,18,27] each containing a single plant, connected by a plastic tube covered at both ends with a thin nylon mesh (50 μm diam. porosity), allowing only hyphae of *R. irregularis* to connect both plants (Figure S1F). In that system, the bacterium inoculated on the mycorrhized plant was able to reach the plant

(C) Epifluorescence pictures of *B. velezensis* biofilm development along *R. irregularis*. Epifluorescence pictures were taken by microscopy 3, 7, 10, and 14 days post inoculation (dpi) of *B. velezensis* GA1 expressing GFP (green color) on 3-month-old *R. irregularis* hyphae (blue arrow). By Fiji image processing, measurement of biofilm thickness was achieved on one side of the hyphae. Five co-culture systems were used (biological replicates), and 4 images per co-culture system were taken at different locations over time (technical replicates). Representative pictures are shown in the figures.

(D) Evolution of *B. velezensis* biofilm thickness along *R. irregularis* hyphae, 3, 7, 10, and 14 dpi. The boxes encompass the 1st and 3rd quartiles, the whiskers extend to the minimum and maximum points, and the midline indicates the median. The individual points represent 5 biological replicates (different shapes) and 3 technical replicates (3 different colors in the same shape). The evolution of the biofilm thickness over time can be followed for each replicate by the same shape and color. $n = 15$; one-way analysis of variance (ANOVA) and Tukey's HSD (honestly significant difference) test ($\alpha = 0.05$): ns, not significant; * $0.01 < p < 0.05$; ** $0.001 < p < 0.01$; *** $0.0001 < p < 0.001$.

(E) Epifluorescence pictures of *B. velezensis* biofilm development along *R. irregularis* hyphae and spores. Left: *B. velezensis* development along branched absorbing structures. Right, *B. velezensis* growth on the surface of spores. Epifluorescence pictures were taken by microscopy, respectively, 3 and 7 dpi of *B. velezensis* GA1 expressing GFP (green color). (F and G) Macroscopic view of the colonization of GFP-tagged strain *B. velezensis* GA1 (green color in epifluorescence) along the hyphal network of *R. irregularis* 3 dpi of *B. velezensis*. Microscopic composite pictures were taken in bright-field channel (F) and in epifluorescence (G). The blue arrow shows the inoculation drop area on the AM fungal hyphal network.

See also Figures S1 and S2 and Videos S1 and S2.

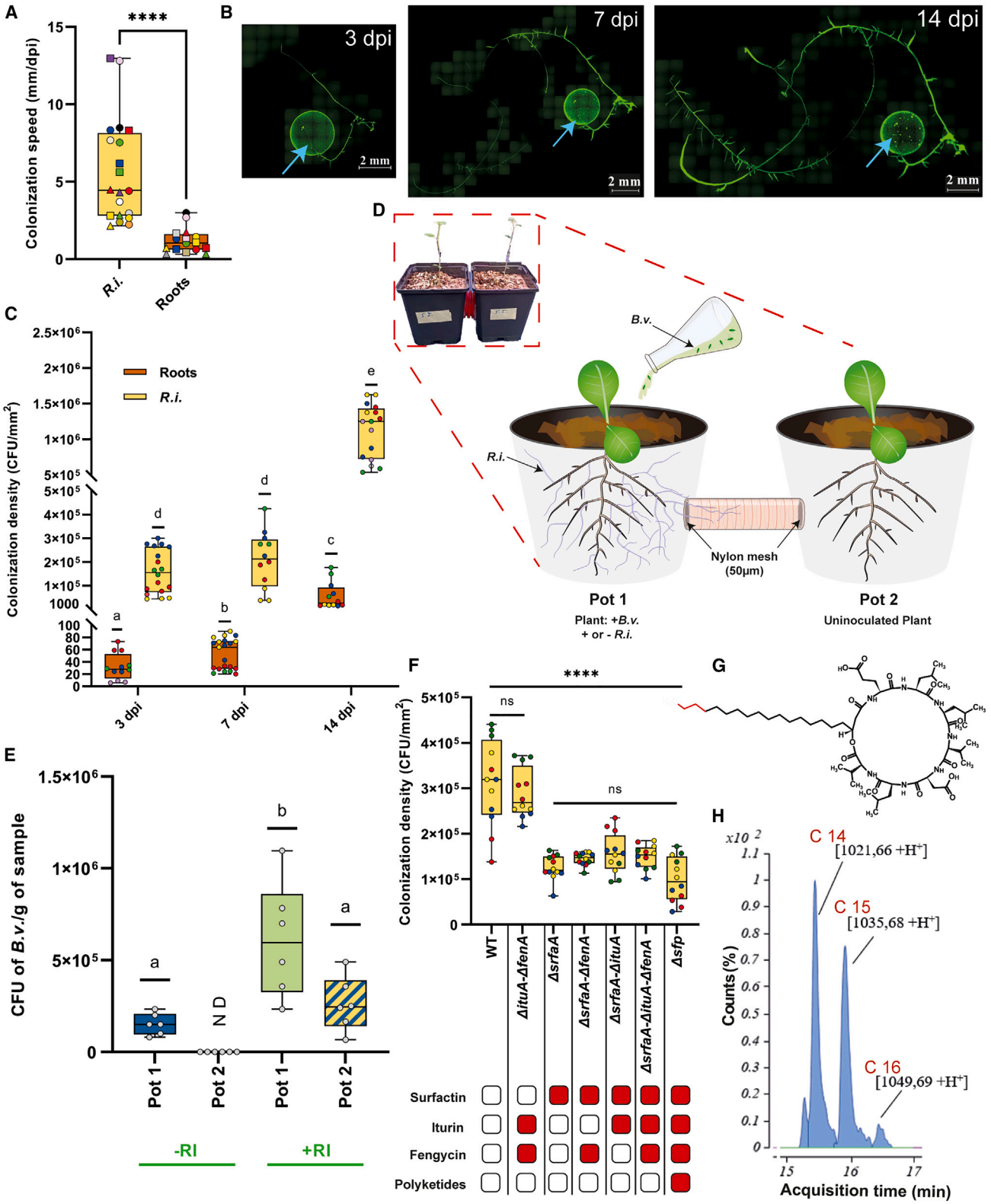

Figure 2. *B. velezensis* colonize effectively AM fungal hyphae compared with root *via* its surfactin production

(A) Colonization speed of *B. velezensis* along hyphae of 3-month-old cultures of *R. irregularis* (*R.i.*: yellow) and along *D. carota* hairy roots (roots: brown) during a time lapse of 14 days. The boxes encompass the 1st and 3rd quartiles, the whiskers extend to the minimum and maximum points, and the midline indicates the median. The individual points represent 7–11 biological replicates (different color) and 1–3 technical replicates corresponding to the speed of colonization taken

(legend continued on next page)

in the other pot only by colonizing the hyphae connecting the two plants (Figure 2E). Selective plate counting of *B. velezensis* among the bacterial community naturally present in the substrate was based on antibiotic resistance and fluorescence of GFP-tagged GA1. *R. irregularis* was quantified by qPCR using a strain-specific house-keeping gene. Data first revealed that plant roots associated with *R. irregularis* (Pot 1 + *R.i.*) exhibited a significantly higher number of GA1 CFUs compared with non-mycorrhized plants (Pot 1 − *R.i.*), indicating that the presence of *R. irregularis* favors *B. velezensis* root colonization also in these conditions (Figure 2E). Moreover, our results showed that *B. velezensis* inoculated on a plant associated with *R. irregularis* (Pot 1 + *R.i.*) was able to colonize a non-bacterized neighboring plant (Pot 2 + *R.i.*) via the common mycorrhizal network connecting both plants. In the control system without *R. irregularis* (Pot 1 − *R.i.*), no bacterial cells were detected on the plant in Pot 2, 20 dpi (Figure 2E). These findings indicate that the association with *R. irregularis* facilitates the transfer of *B. velezensis* cells from one root system to another much faster than expected via passive diffusion.

The surfactin lipopeptide contributes to *B. velezensis* colonization of the hyphosphere

Bacterial fitness can be influenced by secondary metabolites playing key roles in various developmental processes, including motility and biofilm formation.[42–44] Thus, a range of mutants specifically repressed in the synthesis of BSMs were tested in order to determine their role in the AM fungal colonization potential of *B. velezensis*. The bacterial population at the surface of hyphae 7 dpi was significantly reduced for all the knockout mutants unable to produce surfactin family (Figures 2F and 2G). No other non-ribosomal BSMs were involved in hyphal colonization as indicated by the similar loss in colonization ability observed for the *Δsfp* mutant (repressed in 4′-phosphopantetheinyl transferase, which is essential for the proper functioning of non-ribosomal peptide biosynthesis machineries), and other double or triple mutants unable to produce at least surfactin (Figure 2F). In *B. velezensis*, it has been shown that surfactin deficiency causes impaired biofilm formation, the strains becoming unable to colonize roots.[41,45] Based on these data, we wanted to confirm the production of surfactin by *B. velezensis* upon AM fungal colonization. Thus, we generated hyphosphere extracts obtained upon *B. velezensis* colonization of the hyphae in *in vitro* system that were analyzed next by UPLC-qTOF-MS (ultra-high performance liquid chromatography with quadrupole time-of-flight mass spectrometry) optimized for detection of nanomolar amounts, quantification, and structural characterization of non-ribosomal BSMs. Based on exact mass and retention time compared with standards, we observed substantial amounts of surfactin (as a mixture of homologs that differ in the length of the fatty acid chain, Figures 2G and 2H) at concentrations close to the micromolar range (0.605 μM in average at 9 dpi). This confirmed that *B. velezensis* cells in biofilm associated with *R. irregularis* readily secrete this cyclic lipopeptide (CLiP), which significantly contributes to colonization.

B. velezensis associates with *R. irregularis* in a compatible interaction

B. velezensis efficiently colonized the hyphae of *R. irregularis*, but this bacterium is a strong producer of antimicrobials, and we thus wanted to evaluate the impact of *B. velezensis* on hyphae viability. We first measured succinate dehydrogenase (SDH) activity as an indicator of AM fungal viability by histochemical staining[46] (Figure 3A). Image analysis revealed that the enzymatic activity did not differ between non-colonized and colonized hyphae (Figure 3B), indicating that the presence of the bacterium did not influence adversely the respiratory metabolism of *R. irregularis*. We also monitored by time-lapse microscopy imaging, the impact

at different time point (measured 3 dpi: circle shape, 7 dpi: square shape, and 14 dpi: triangle shape) (days post inoculation [dpi]). The evolution of the speed of colonization over time can be followed for each replicate with the same color. $12 \leq n \leq 24$; Student's t test ($\alpha = 0.05$): **** $p < 0.0001$.

(B) *B. velezensis* colonization along hyphae of 3-month-old cultures of *R. irregularis* overtime. Microscopic composite pictures were taken in epifluorescence. The blue arrow shows the inoculation drop area on the AM fungus hyphal network. The speed colonization is quantified by the measurement of the distance traveled by *B. velezensis* (green color) from the inoculation drop (blue arrow) divided by the dpi.

(C) Colonization density of hyphae of 3-month-old *R. irregularis* cultures (*R.i.*: yellow) or transformed roots of *D. carota* cultures (roots: brown) 3, 7, and 14 dpi of *B. velezensis* The boxes encompass the 1st and 3rd quartiles, the whiskers extend to the minimum and maximum points, and the midline indicates the median. The individual points represent 4 at 6 biological replicates (different color) and 1 at 6 technical replicates (same color). $12 \leq n \leq 21$; one-way analysis of variance (ANOVA) and Tukey's HSD (honestly significant difference) test ($\alpha = 0.05$). Groups with different letters differed significantly from each other.

(D) Picture (red square) and schematic view of the experimental design in which two plants of *Solanum tuberosum* (pot 1 and pot 2) were connected by a tube with both ends closed with a nylon mesh of 50 μm porosity. The nylon barrier prevented the passage of roots. During the planting, pot 1 was inoculated (+*R.i.*) or not (−*R.i.*) with *R. irregularis*. After 5 months of growth, the plants associated or not with *R. irregularis* in pot 1 were inoculated with *B. velezensis*. The plants in pot 2 were not inoculated with any microorganisms.

(E) Bacterial population of GFP-tagged strain *B. velezensis* GA1 quantified by plate-counting of colony-forming units (CFUs) by gram of sample, 10 dpi. All the plants in pot 1 associated (+*R.i.*) or not (−*R.i.*) with *R. irregularis* were inoculated with *B. velezensis*. Plants in pot 2 were not inoculated with any microorganisms. The boxes encompass the 1st and 3rd quartiles, the whiskers extend to the minimum and maximum points, and the midline indicates the median. The individual points represent 6 biological replicates (6 different systems). $n = 6$; one-way analysis of variance (ANOVA) and Tukey's HSD test ($\alpha = 0.05$). Groups with different letters differed significantly from each other. ND, no detected.

(F) Colonization density of hyphae of 3-monts-old *R. irregularis* cultures 7 dpi of *B. velezensis* wild type (WT) and mutants unable to produce one or several bioactive secondary metabolites (BSMs). Metabolites not produced by the different mutants are illustrated with red boxes in the table below. The boxes encompass the 1st and 3rd quartiles, the whiskers extend to the minimum and maximum points, and the midline indicates the median. The individual points represent 4 biological replicates (different color) and 3 technical replicates (same color). $n = 12$; one-way analysis of variance (ANOVA) and Tukey's HSD test ($\alpha = 0.05$). ns, not significant; **** $p < 0.0001$.

(G) Structure of surfactin composed of a peptidic moiety linked to a fatty acid tail (ranging from 12 to 16 carbons, red part).

(H) UPLC-MS extract ion chromatogram (EIC) illustrating the relative abundance of surfactin (blue) secreted by *B. velezensis* 9 dpi on hyphae of a 3-month-old *R. irregularis* culture. The different peaks correspond to the structural variants differing in fatty acid chain length (surfactin, C14 to C16), and the number in red represents the length of the fatty acid tail.

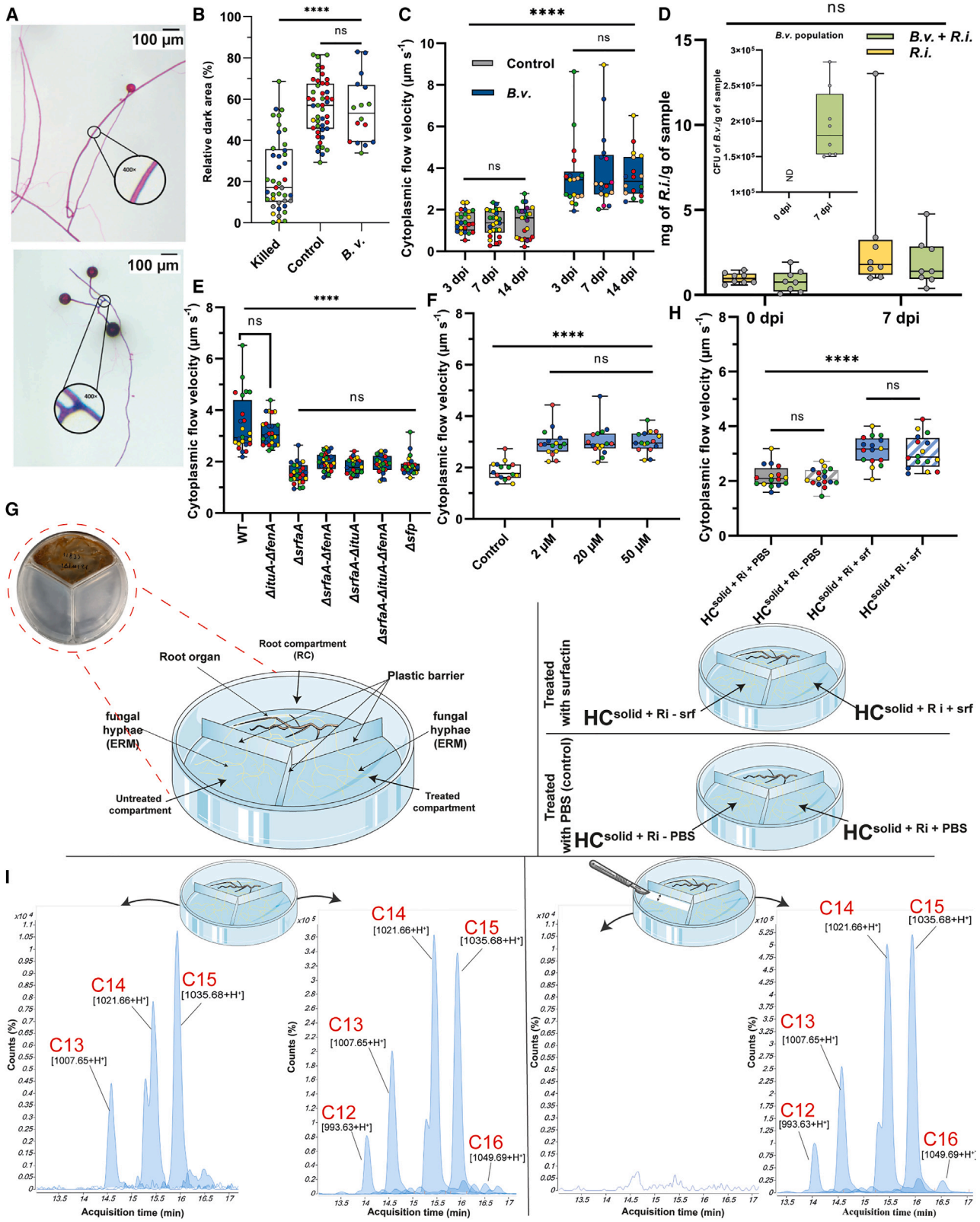

Figure 3. Viability of *R. irregularis* and cytoplasmic streaming within hyphae upon colonization by *B. velezensis*

(A) Histochemical determination of succinate dehydrogenase (SDH) activity indicating respiratory metabolism of *R. irregularis* hyphae. (Bottom) Control (with physiological water) showing dark blue-violet zones corresponding to SDH activity. (Top) Killed hyphae (with formaldehyde) showing pink color corresponding to

(legend continued on next page)

of *B. velezensis* on the cytoplasmic flow within hyphae, which is considered as functional trait of AM fungi, allowing the translocation of resources from plant to fungus and vice versa and somehow reflecting fungal vitality[26,47,48] (Videos S3, S4, and S5). Flow velocity inside non-colonized (Video S4) or colonized hyphae (Video S3) remained stable over time, as observed at 3 and 14 dpi. However, the presence of the bacterium increased the cytoplasmic flow velocity compared with non-colonized hyphae whatever the time of observation (Figure 3C). Thus, *B. velezensis* colonization did not affect fungal fitness, which agrees with the fact that the presence of the bacterium does not cause a reduction of the AM fungal population *in planta* (Figure 3D).

Secondary metabolites and more particularly CLiPs are key components involved in multitrophic interactions established by *Bacillus* in the rhizosphere.[29,49] We thus investigated their possible role in the increase of cytoplasmic flow velocity triggered by the bacterium in *R. irregularis* hyphae. We first analyzed *B. velezensis* GA1 mutants deleted in CLiP-biosynthesis genes. Co-cultivation with *R. irregularis* of all mutants impaired in surfactin production did not result in increased flow velocity, providing the first strong evidence for the crucial role of this CLiP but not iturin, fengycin, or any other non-ribosomal compounds (Figure 3E). As an important proof, we added purified surfactin to monocultures of *R. irregularis* associated to *D. carota* and observed a similar trend on flow velocity upon treatment with concentrations as low as 2 μM, which is in the range of the amounts detected in the hyphosphere (Figure 3F). In order to determine if this response is restricted to hyphae segments in contact with the lipopeptide or not, we next used a tri-compartmented culture system in which the hyphal network, but not the root, is allowed to cross into two different hyphal compartments physically separated by a plastic barrier,[26] thereby preventing surfactin from diffusing between the compartments (Figure 3G). With this setup, we observed the diffusion of the response within the ERM and across the root compartment. The effects of surfactin were not limited to hyphae in the treated compartment ($HC^{solid + Ri + srf}$) but also influenced distal regions (Figure 3H), resulting in an overall increase in cytoplasmic flow observed in the untreated compartment ($HC^{solid + Ri - srf}$) at 48 h post inoculation (Figures 3H and S3). These data strongly suggest that surfactin acts as a trigger driving the AMF to systemically boost its cytoplasmic translocation. Interestingly, UPLC-qTOF MS analyses of hyphosphere extracts prepared from the untreated compartment ($HC^{solid + Ri - srf}$) revealed that surfactin was translocated at distal zone through the ERM (Figure 3I) since significant amounts (corresponding to 0.32 μM in

dead hyphae. Pictures of stained hyphae of a 3-month-old culture of *R. irregularis* were taken with the stereomicroscope. The images presented are representative examples selected from independent samples repeated on minimum 3 biological replicates.

(B) Relative dark area corresponds to potential SDH activity of *R. irregularis* colonized by *B. velezensis* (*B.v.*) 14 dpi along hyphae of 3-month-old cultures of *R. irregularis*, compared with killed hyphae (with formaldehyde 2%) and the control (treated with physiological water). The boxes encompass the 1st and 3rd quartiles, the whiskers extend to the minimum and maximum points, and the midline indicates the median. The individual points represent 3–5 biological replicates (different colors) and 1–20 technical replicates (same colors). $16 \leq n \leq 47$; one-way analysis of variance (ANOVA) and Tukey's HSD (honestly significant difference) test ($\alpha = 0.05$): ns, not significant; **** $p < 0.0001$.

(C) Cytoplasmic flow velocity in hyphae of *R. irregularis* in presence or absence of GFP-tagged *B. velezensis* measured 3, 7, and 14 dpi. The boxes encompass the 1st and 3rd quartiles, the whiskers extend to the minimum and maximum points, and the midline indicates the median. The individual points represent 4–8 biological replicates (different colors) and 4–6 technical replicates (same colors). $18 \leq n \leq 24$; one-way analysis of variance (ANOVA) and Tukey's HSD test ($\alpha = 0.05$): ns, not significant; **** $p < 0.0001$.

(D) Fungal population of *R. irregularis* (*R.i.*) quantified by quantitative PCR reported by gram of roots sampled with attached substrate (mg of *R.i.*/g of sample), 0 and 7 dpi of plants treated with inoculum of *B. velezensis* (*B.v.* + *R.i.*, green), or with a solution without any microorganism (*R.i.*, yellow). The boxes encompass the 1st and 3rd quartiles, the whiskers extend to the minimum and maximum points, and the midline indicates the median. The individual points represent 8 biological replicates (8 different plants). $n = 8$; one-way analysis of variance (ANOVA) and Tukey's HSD test ($\alpha = 0.05$): ns, not significant. Inside the graph is included the bacterial population of *B. velezensis* in the treatment combining *B. velezensis* and *R. irregularis* (*B.v.* + *R.i.*, green), before the inoculation of the bacterium and 7 dpi of *B. velezensis*.

(E) Cytoplasmic flow velocity in hyphae of *R. irregularis*. in presence of *B. velezensis* wild-type (WT) or knockout mutants, 7 dpi along hyphae. The boxes encompass the 1st and 3rd quartiles, the whiskers extend to the minimum and maximum points, and the midline indicates the median. The individual points represent 4 biological replicates (different colors) and 6–7 technical replicates (same colors). $24 \leq n \leq 25$; one-way analysis of variance (ANOVA) and Tukey's HSD test ($\alpha = 0.05$): ns, not significant; **** $p < 0.0001$.

(F) Cytoplasmic flow velocity in hyphae of *R. irregularis* in contact with increasing concentrations of pure surfactin (2, 20, or 50 μM) compared with a PBS control. The boxes encompass the 1st and 3rd quartiles, the whiskers extend to the minimum and maximum points, and the midline indicates the median. The individual points represent 4 biological replicates (different colors) and 4 technical replicates (same colors). $n = 16$; one-way analysis of variance (ANOVA) and Tukey's HSD test ($\alpha = 0.05$): ns, not significant; **** $p < 0.0001$.

(G) Picture (red circle) and illustration of a tri-compartmented experimental setup. In one compartment (root compartment [RC]) roots of *D. carota* are associated to *R. irregularis*, from which the hyphae colonize two side compartments. One side compartment contained either pure surfactin at a concentration of 2 μM ($HC^{solid + Ri + srf}$) or PBS ($HC^{solid + Ri + PBS}$). The other side compartment, not supplemented with surfactin or PBS, was annotated as follows ($HC^{solid + Ri - srf}$ or $HC^{solid + Ri - PBS}$). A plastic barrier prevents surfactin from diffusing between compartments.

(H) Cytoplasmic flow velocity in the compartment treated with surfactin ($HC^{solid + Ri + srf}$, blue) or PBS ($HC^{solid + Ri + PBS}$, gray) and in their untreated associated compartment for surfactin ($HC^{solid + Ri - srf}$, blue stripes) or for PBS ($HC^{solid + Ri - PBS}$, gray stripes). The boxes encompass the 1st and 3rd quartiles, the whiskers extend to the minimum and maximum points, and the midline indicates the median. The individual points represent 4 biological replicates (different colors) and 4 technical replicates (same colors). $n = 16$; one-way analysis of variance (ANOVA) and Tukey's HSD test ($\alpha = 0.05$): ns, not significant; **** $p < 0.0001$.

(I) Illustration of the tri-compartmented experimental setup in which surfactin was added to one hyphal compartment (treated compartment), keeping the same amount of surfactin 19.16 μM in average ($n = 3$) than the concentration used to the treatment (20 μM). In the second compartment, the amount of surfactin was quantified when the ERM was intact (left) or when the network was cut by a band of 0.5 cm width (right) to evaluate if surfactin may be translocated by *R. irregularis*. Representative UPLC-MS extract ion chromatogram (EIC) illustrating the relative abundance of surfactin (blue) in each compartment, and the number in red represents the length of the fatty acid tail. *D. carota* transformed roots were confined to the root compartment (RC), but the fungus was able to cross the plastic barrier, entering the hyphal compartments (HCs). Another plastic barrier prevented the transfer of surfactin between the two HC.

See also Figure S3 and Videos S3, S4, and S5.

average) were recovered from the $HC^{solid + Ri - srf}$ when the ERM was intact but no trace of the lipopeptide could be detected when the mycelium network was cut. These results underlined the potential of the AMF to transport this bacterial secondary metabolite through its network.

Attenuated fengycin production in the hyphosphere prevents *B. velezensis* from antagonizing *R. irregularis*

B. velezensis is a strong producer of antifungal BSMs, including iturin- and fengycin-type CLiPs, which are well described for their activity against a wide range of fungal plant pathogens.[29,50,51] In order to understand how *R. irregularis* may coexist with this antagonistic bacterium, we tested the toxicity of pure CLiPs on the fungus. We used propidium iodide (PI) staining as indicator of membrane integrity since the toxicity of these molecules mainly relies on their pore-forming activity in biological membranes causing cytosolic leakage and death of target cells.[52–54] Fengycin and iturin did not impact hyphae membrane integrity at 2 μM, while at 20 and 50 μM, fengycin markedly destabilized the membranes and iturin only at the highest concentration (50 μM) (Figures 4A and 4B). In contrast, surfactin did not affect membrane integrity over the tested concentration range (Figure 4B).

Next, we wanted to evaluate the production of these compounds in the hyphosphere upon AM fungal colonization. CLiP profiling via UPLC-qTOF-MS revealed a distinct pattern compared with the one observed upon growth in lab media or in a medium mimicking plant exudates[55] (Figure 4C). Upon growth in rich optimized lab media, *B. velezensis* typically secretes CLiPs in relative proportions of approximately 50% surfactin, 25% iturin, and 25% fengycin.[55] However, the hyphosphere samples exhibited different ratios, with surfactin accounting for 60% (±11.21%) and iturin for 36.5% (±10.20%), while fengycin was present in minimal amounts of only 1.5% (±0.78%) (Figure 4D). The amounts recovered corresponded approximately to 0.61 μM ± 0.21 for surfactin, 0.48 μM ± 0.016 for iturin, and 0.03 μM ± 0.001 for fengycin. Similar relative CLiPs proportions were observed when *B. velezensis* planktonic cells were cultured in presence of exudates collected from AM fungal hyphae as sole nutrient source (surfactin: 2.73 μM ± 1.04; iturin: 1.86 μM ± 1.06; fengycin: 0.0478 μM ± 0.0325), indicating that the reduced fengycin production is not related to biofilm formation and is not contact-dependent (Figure 4D). Also, data presented in Figure 4B show that at these concentrations, fengycin is not cytotoxic for the fungus. Since the nature of carbon sources in the medium may influence BSM production by *Bacillus* spp.,[55–57] we postulated that modulation of the CLiP patterns in the hyphosphere could be driven by the specific nutritional context offered by the hyphae exudates. To simulate this context, we developed a minimal medium called AMF exudate mimicking medium (AMF-EMM) that only contains oligo-elements and the carbon sources typically encountered in hyphal exudates.[13–15] Cultivating *B. velezensis* in this medium resulted in a significant increase in the relative proportions of fengycin and surfactin compared with natural exudates (Figure 4D). Therefore, we assume that the CLiP pattern produced by *B. velezensis* upon interaction with *R. irregularis* and characterized by very low amounts of harmful fengycin is not due to specific nutritional context but is formed in response to the perception of some unidentified signal(s) secreted by the AMF.

B. velezensis produces antimicrobials inhibiting soilborne competitors

Our data in Figure 4 indicate that *B. velezensis* developing as biofilm on AM fungal hyphae still efficiently produces CLiPs and potentially other antimicrobial secondary metabolites. Therefore, we next wanted to assess if some compounds actively secreted by the bacterium could protect AMF against potentially harmful competitors such as *Trichoderma harzianum* and *Collimonas fungivorans*.[58,59] We first evaluated the growth inhibitory activity of the crude cell free supernatant (CFS) obtained after growth of *B. velezensis* in AM fungal exudates toward *T. harzianum* and *C. fungivorans* and observed a significant antagonistic effect of the CFS from wild-type GA1 on both species (Figures 5A and 5B). We next tested mutants of *B. velezensis* unable to produce those BSMs that are readily formed by GA1 wild type upon growth in the hyphosphere. A complete loss of anti-*Trichoderma* activity was observed by testing CFS extracts obtained from the mutants *ΔbacA* and *ΔsfpΔbacA* repressed in the synthesis of the non-ribosomal SFP-independent di-peptide bacilysin (Figure 5A). The crucial role of bacilysin in the antifungal activity developed by *B. velezensis* against *T. harzianum* was further supported by the similar activity of the *Δsfp* mutant unable to form the other non-ribosomal products CLiPs and polyketides (Figure 5A). Significant amounts of bacilysin were detected in hyphosphere extracts from AMF colonized by *B. velezensis* (Figure 5C), indicating that this compound was readily formed by the bacterium while growing on the fungus. Results with mutants repressed in the synthesis of antifungal CLiPs known for their individual or synergistic antifungal activity demonstrated the reduced role of these metabolites against *T. harzianum* within the hyphosphere context (Figure S4A). The outcome of the interaction between *Trichoderma* sp. and *B. velezensis* may vary from mutualism to antagonism depending on many factors.[60] In the context of antagonism, previous research has highlighted the significance of iturin production by *B. velezensis* in inhibiting the growth of *Trichoderma* spp.[61] However, we assume that in our conditions, the concentration of iturin in the hyphosphere did not reach the level necessary to affect the development of this mycoparasite. Regarding *C. fungivorans*, none of the knockout mutants showed a significant loss in the antibacterial activity observed for the wild type (Figures 5B and S4B). Conserved anti-*Collimonas* activity in Δ*sfp* and Δ*sfp*Δ*bacA* extracts suggests the involvement of additional ribosomal compound(s) that remains to be identified.

B. velezensis and *R. irregularis* interaction provides enhanced ISR functionality

Altogether, our results show that *B. velezensis* and *R. irregularis* establish a mutualistic partnership, but whether their association may result in an enhanced functionality in terms of protection of their host plant against pathogen ingress or not has not been investigated so far. Therefore, we wanted to test in greenhouse trials whether the combination of these two plant-beneficial microbes is able to protect tomato plants (*Solanum lycopersicum*, used as model for *Solanaceae*) from disease caused by *Botrytis cinerea*, a major pathogen in a wide range of crops.[62,63] We

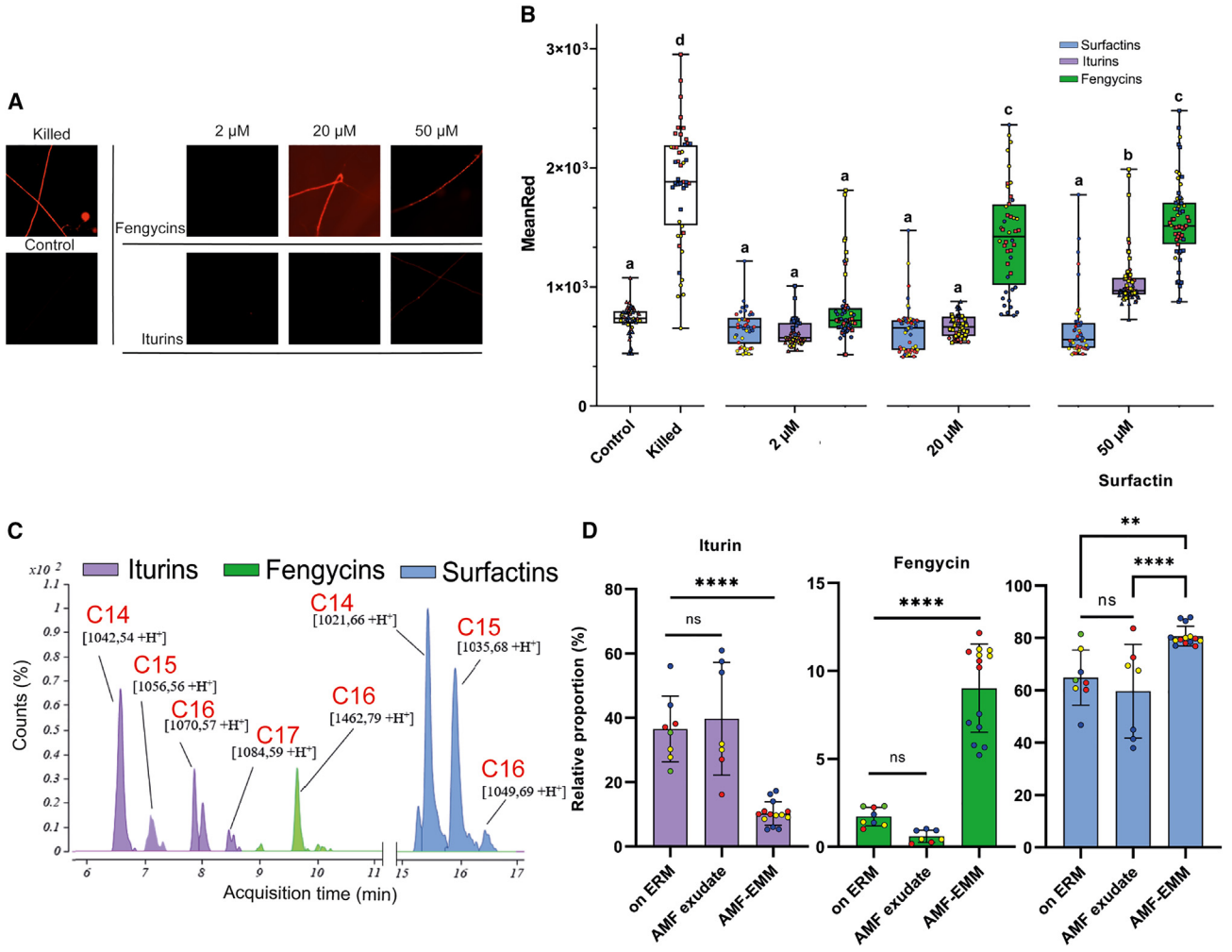

Figure 4. Effect of *B. velezensis* antifungal compounds on *R. irregularis* and their modulation through *R. irregularis* exudates

(A and B) *R. irregularis* hyphae stained with 50 µg mL^{-1} PI after treatment with 2, 20, or 50 µM of fengycin, iturin, or surfactin. AM fungal hyphae treated with PBS solution (control) and 1% Triton X-100 with 2% formaldehyde (killed) were used as controls. (A) PI cell staining of *R.i.* hyphae observed by fluorescence microscopy. (B) Dose effect of pure fengycin (green), iturin (purple), and surfactin (blue) produced by *B. velezensis* on membrane integrity of 3-month-old (triangle shape), 5-month-old (square shape), or 6-month-old (circle shape) hyphae of *R. irregularis* cultures measured by fluorescence upon staining with PI. High MeanRed values mean high membrane permeabilization. The boxes encompass the 1st and 3rd quartiles, the whiskers extend to the minimum and maximum points, and the midline indicates the median. The individual points represent 3 biological replicates (different colors) and 9–26 technical replicates (same colors). The dose effect of fengycin, iturin, and surfactin has been evaluated according to different ages of *R. irregularis* cultures (different shapes). $43 \leq n \leq 65$; letters a–d indicate statistically significant differences according to one-way analysis of variance (ANOVA) and Tukey's HSD (honestly significant difference) test ($\alpha = 0.05$).

(C) UPLC-MS extract ion chromatogram (EIC) illustrating the relative abundance of surfactin (blue), iturin (purple), and fengycin (green) family secreted by *B. velezensis* 9 dpi on hyphae of 3-month-old cultures of *R. irregularis*. The different peaks for each CLiP correspond to the structural variants differing in fatty acid chain length. The number in red represents the length of the fatty acid tail for each BSM.

(D) Relative surfactin (blue), iturin (purple), and fengycin (green) proportions corresponding to the detected peaks areas of each CLiP compared with the total amount of the 3 families of CLiPs following growth condition. CLiPs relative proportion when *B. velezensis* evolved along AM fungal hyphae (on ERM), on exudates collected from AM fungal hyphae (AM fungal exudate), on AM fungal exudates mimicking medium (AMF-EMM). Bars represent the mean ± SD of 3–4 biological replicates (different colors) and 2–4 technical replicates (same colors). $7 \leq n \leq 14$; letters a–d indicate statistically significant differences according to one-way analysis of variance (ANOVA) and Tukey's HSD test ($\alpha = 0.05$): ns, not significant; ** $0.001 < p < 0.01$, **** $p < 0.0001$.

specifically evaluated the protective effect due to ISR since the beneficial microbes were inoculated at the root level while infection by *B. cinerea* was performed on leaves and rated based on the size and number of spreading necrotic lesions. This spatial separation was maintained throughout the experiment because no trace of *Bacillus* was observed in leaf tissues at the time of infection (no typical fluorescent colonies with a detection limit < 10^3 CFU/g fresh weight, data not shown). This indicates that the bacterium has not migrated from roots to shoots, allowing to exclude direct antagonism toward the pathogen. Data showed a strong decrease in both disease severity (approx. 60%) and disease incidence (approx. 75%) in plants co-inoculated with *R. irregularis* and *B. velezensis* compared with controls. Treatments with the AMF or the bacterium alone provided

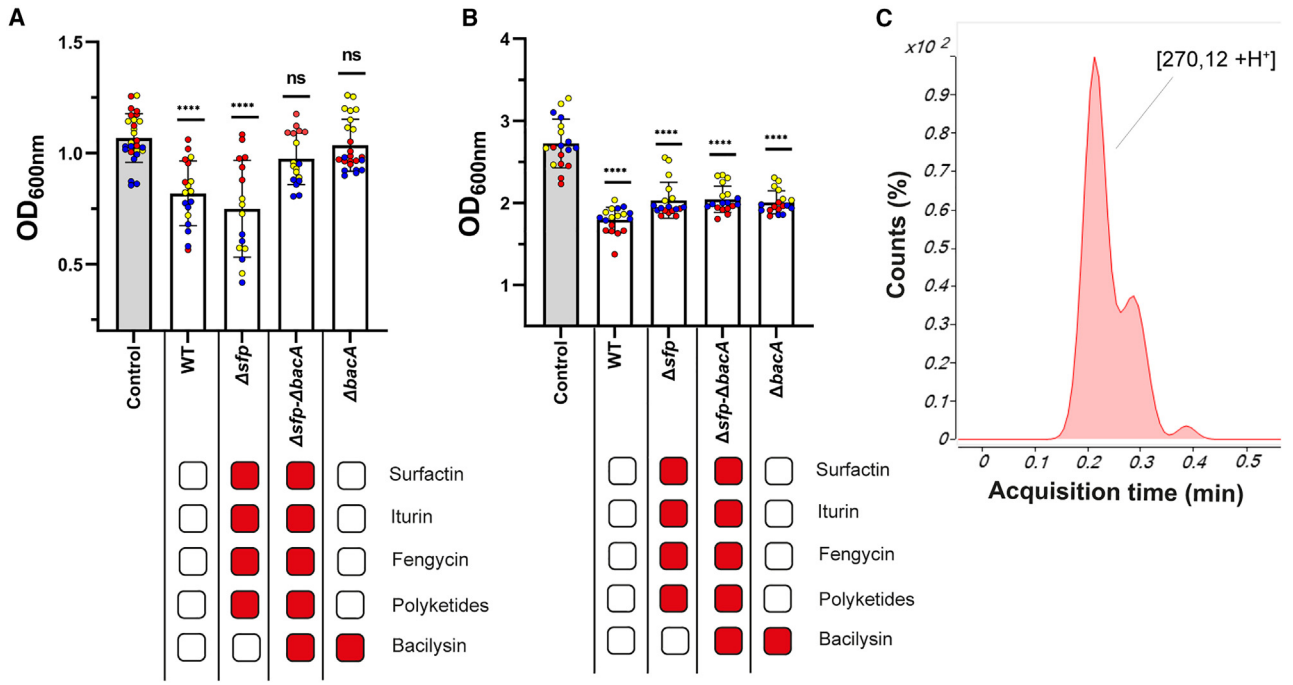

Figure 5. BSMs produced by *B. velezensis* in the hyphosphere of *R. irregularis* allowing an antagonism activity against *Trichoderma harzianum* and *Collimonas fungivorans*

(A) Effect of *B. velezensis* GA1 wild-type or mutant cell-free supernatants (CFSs), produced on exudates of *R.i.* cultures, on the growth of *Trichoderma harzianum* Rifai MUCL 29707. The optical density (OD_{600nm}) of the fungi was measured after 36 h of growth in the presence or absence (control) of CFS. Metabolites not produced by the different mutants are illustrated with red boxes in the table below. Bars represent the mean ± SD of 3 biological replicates (different colors) and 4–9 technical replicates (same colors). $16 \leq n \leq 27$, one-way analysis of variance (ANOVA) and Dunnett's test ($\alpha = 0.05$): ns, not significant; **** $p < 0.0001$.

(B) Effect of GA1 wild-type or mutant cell-free supernatants (CFSs) produced on exudates of *R.i.* cultures on the growth of *Collimonas fungivorans* LMG 21973. The optical density ($OD_{600\ nm}$) of the bacterium was measured after 24 h of growth in the presence or absence (control) of CFS. Metabolites not produced by the different mutants are illustrated with red boxes in the table below. Bars represent the mean ± SD of 3 biological replicates (different colors) and 6 technical replicates (same colors). $16 \leq n \leq 27$, one-way analysis of variance (ANOVA) and Dunnett's test ($\alpha = 0.05$) compared with the control: ns, not significant; **** $p < 0.0001$.

(C) UPLC-MS extract ion chromatogram (EIC) illustrating the relative abundance of bacilysin (red), secreted by *B. velezensis* 9 dpi on 3-month-old *R.i.* cultures. See also Figure S4.

some protection but to a significantly lower level (Figures 6A and 6B). Monitoring of microbial population in soil of co-inoculated plants (as described in Figure 2D) revealed that the AM fungal density remained stable overtime while *B. velezensis* CFUs markedly increased within 2 weeks (Figures 6C and 6D). This confirmed first that the bacterium does not negatively impact AM fungal population and second that the presence of *Rhizophagus* may favor *Bacillus* soil invasion. Moreover, inoculation with both microorganisms did not impact plant size compared with controls (Figure 6E), strongly suggesting that enhanced disease resistance is not indirectly due to a higher robustness. From all these data, we infer that mutualistic cooperation between *R. irregularis* and *B. velezensis* confers an increased potential for immune activation in tomato plants, thereby resulting in higher resistance.

DISCUSSION

In most instances, cross-kingdom interactions between plant beneficial rhizobacteria and soilborne fungi result in antagonistic outcomes and fungal growth inhibition due to production of secondary metabolites with fungicidal activity.[29,64,65] Here we unveil a rather novel unanticipated compatibility between *B. velezensis* as strong bacterial competitor and *R. irregularis* as keystone AM fungal species, ensuring a stable coexistence and partnership. *Bacillus* spreading along the mycelia of various fungi and oomycetes has been already reported[19,66,67] but this work provides unique insights into the mutualistic interaction established between a biocontrol strain and AM fungi. *B. velezensis* dwelling in the hyphosphere efficiently produces iturin-type lipopeptides known for their strong antifungal properties against a wide range of phytopathogens[50,68–70] but which appears not toxic to *R. irregularis* at the concentrations tested (2–20 μM). In general, the biological activity of lipopeptides is mainly related to their ability to interact with the cell membrane of the target organism, which depends both on the structure of the molecule and on the lipid composition and organization of the target membrane.[52–54] AM fungal membranes are mainly constituted of 24-methyl cholesterol and phosphatidylinositol/phosphatidylcholine with saturated and/or monounsaturated fatty acids as phospholipids, which widely differ from lipid compositions of pathogenic fungi membranes.[71–73] Therefore, we assume that the low toxicity of iturin to *R. irregularis* is due to the specific lipid content within the plasma membrane of AM fungal hyphae. In contrast to iturin,

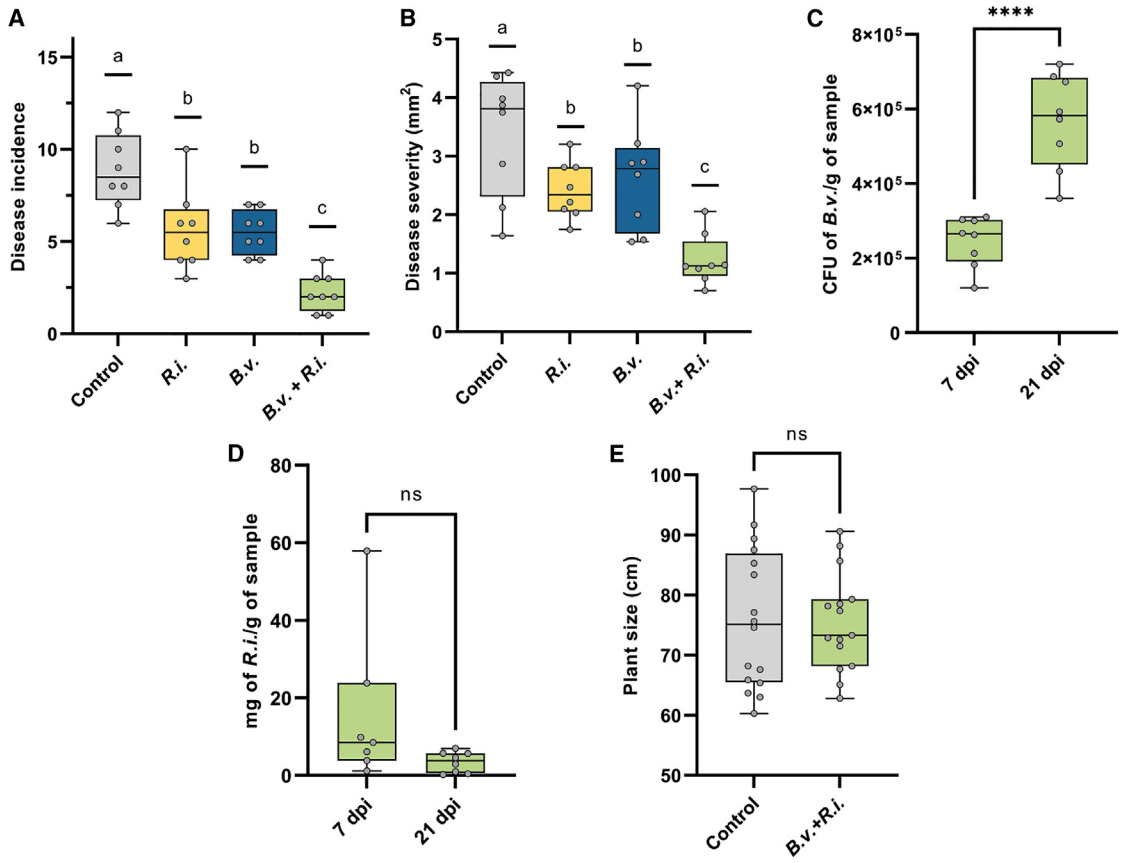

Figure 6. Interaction between *B. velezensis* and *R. irregularis* increases plant protection

(A) Number of emerging/spreading lesions (disease incidence) 21 days after infection with *B. cinerea* evaluated on 15 leaves of 8 *S. lycopersicum* plants treated with *R. irregularis* (*R.i.*, yellow), *B. velezensis* (*B.v.*, blue), the combination of both (*R.i.* + *B.v.*, green), or with Hoagland solution as control (gray). The boxes encompass the 1st and 3rd quartiles, the whiskers extend to the minimum and maximum points, and the midline indicates the median. The individual points represent 8 biological replicates. $n = 8$; letters a–c indicate statistically significant differences according to one-way analysis of variance (ANOVA) and Tukey's HSD (honestly significant difference) test ($\alpha = 0.05$).

(B) Size of emerging lesions (disease severity) quantified by ImageJ Fiji, 21 days after infection with *B. cinerea* on leaves of *S. lycopersicum* plants treated with *R. irregularis* (*R.i.*), *B. velezensis* (*B.v.*), the combination of both (*R.i.* + *B.v.*, green), or with Hoagland solution as control. The boxes encompass the 1st and 3rd quartiles, the whiskers extend to the minimum and maximum points, and the midline indicates the median. The individual points represent 8 biological replicates. $n = 8$; letters a–c indicate statistically significant differences according to one-way analysis of variance (ANOVA) and Tukey's HSD test ($\alpha = 0.05$).

(C) Bacterial population of GFP-tagged strain *B. velezensis* GA1 quantified by plate-counting of colony-forming units (CFUs) reported by gram of roots sampled with attached substrate (CFU of *B.v.*/g of sample), 7 and 21 dpi of the bacterium on *S. lycopersicum* roots associated with *R. irregularis* (*B.v.* + *R.i.*, green). The boxes encompass the 1st and 3rd quartiles, the whiskers extend to the minimum and maximum points, and the midline indicates the median. The individual points represent 8 biological replicates. $n = 8$; Student's t test ($\alpha = 0.05$): **** $p < 0.0001$.

(D) Fungal population of *R. irregularis* quantified by quantitative PCR reported by gram of roots sampled with attached substrate (mg of *R.i.*/g of sample), 7 and 21 dpi of the bacterium on *S. lycopersicum* plants treated with the combination *R. irregularis* and *B. velezensis* (*B.v.* + *R.i.*, green). The boxes encompass the 1st and 3rd quartiles, the whiskers extend to the minimum and maximum points, and the midline indicates the median. The individual points represent 8 biological replicates. $n = 8$; Student's t test ($\alpha = 0.05$): ns, not significant.

(E) Tomato plant size treated with *R. irregularis* associated with *B. velezensis*, 7 dpi of the bacterium (before treatment with *B. cinerea*) compared with the control treated with Hoagland solution. The boxes encompass the 1st and 3rd quartiles, the whiskers extend to the minimum and maximum points, and the midline indicates the median. The individual points represent 16 biological replicates. $n = 16$; Student's t test ($\alpha = 0.05$): ns, not significant.

our data reveal that fengycin exhibits antagonistic activity at low micromolar concentration on AM fungal hyphae such as reported for many phytopathogenic fungi.[51,74,75] However, production of this CLiP by *B. velezensis* in the hyphosphere is very low, and the compound does not accumulate at inhibitory amounts in the vicinity of AM fungal hyphae. Based on our results, we postulate that fengycin synthesis is dampened in response to the perception of some signal emitted by *R. irregularis*. Beyond their role as nutrients supporting bacterial growth, some carbohydrates and carboxylates secreted by the AM fungi have been described as signals triggering phenotypic and metabolic responses in bacteria.[21,76] However, this is obviously not the case here since growing *B. velezensis* in artificially reconstituted medium containing the typical sugars, organic acids, and amino acids exuded by *R. irregularis* does not lead to such fengycin repression. Other AM fungal-secreted compounds may putatively function as signals such as effector proteins/peptides or plant-derived metabolites such as methyl

salicylate known to be involved in plant-microbe cross-talk.[4,7,77,78] However, none of these compounds could be detected upon UPLC-MS analysis of exudates collected from *R. irregularis* cultures. Resolving the chemical nature of the *R. irregularis* signaling molecule(s) responsible for fengycin modulation thus deserves further investigation, but still, in a broader context, our observation paves the way to the discovery of AM fungal compounds driving cross-kingdom interactions. Our understanding of the external biotic signals that modulate the synthesis of BSMs in *Bacillus* spp. is still limited,[29,51] and this study highlights AM fungi as unique soil-dwelling microbes that may impact CLiP production.

Our findings also provide insights into the molecular basis driving mutualism between the two microbes. The lipopeptide surfactin plays a key role in this interaction since it not only contributes to efficient hyphosphere invasion (by favoring motility and biofilm formation) as reported for root colonization,[31,79,80] but it also acts as trigger enhancing *Rhizophagus* cytoplasmic flow and hence, potentially its functionality. This represents a new natural function for this lipopeptide as signal mediating interkingdom interactions even if deciphering the mechanistic of surfactin perception by the AMF requires further investigation. However, based on the similarity of membrane lipids between AM fungi and plants, we hypothesize that it may rely on a specific interaction with the lipid phase of the AM fungal plasma membrane by analogy with what is observed for interactions with plant cells in the context of immunity stimulation.[31,81–83] Interestingly, surfactin in its canonical form is ubiquitously synthesized by all species belonging to the *B. subtilis* group that are widespread in soil. Other structurally related CLiPs are produced by other rhizobacteria such as *Pseudomonas*.[84,85] This suggests that this type of cross-kingdom communication mediated by CLiPs may have a more global distribution belowground.

Our *in vitro* data further indicate that *B. velezensis* readily uses hyphal exudates to eavesdrop on the AMF and fuel its catabolism to sustain growth and form robust biofilm as described for other bacterial species in interaction with other fungi.[15,76,86–88] *B velezensis* also promptly invades the hyphosphere in a process more efficient than rhizosphere colonization. This was observed with four different *Rhizophagus* species, indicating that *B. velezensis* seems to be well adapted to live in association with AM fungi even if this concept needs to be extended to other fungal genera.[14] Even though they are not considered as members of the core hyphosphere microbiome, some bacilli have been recurrently identified as dominant components within the bacterial community associated with AM fungi.[16,89–93] This suggests that some species like *B. velezensis* underwent specific adaptation during evolution, allowing it to thrive in a lifestyle compatible with AM fungi.

Efficient colonization of ERM provides clear ecological advantages to the bacterium. First, biofilm formation is an essential trait that protects the cell community against abiotic stresses as well as against infiltration by competitors or toxins via the shield effect of the hydrophobin layer.[36,94,95] Secondly, by using the large and dense hyphal networks of AM fungi as dynamic support for biofilm establishment and expansion, *B. velezensis* may extend in a volume of soil inaccessible to roots and thus considerably enhance its invasiveness and persistence in the niche. As described by Kohlmeier et al. with *Fusarium oxysporum* and *Rhexocercosporidium* sp. in interaction with several bacteria,[96] *Bacillus* uses the ERM as fungal highway to facilitate its invasiveness. Bacterial migration along AM fungal hyphae over significant distances has been only recently demonstrated for the phosphate-solubilizing bacteria *Rhanella aquatilis*.[23] Here we provide a first strong evidence on spatiotemporal dynamics of hyphal invasion by *B. velezensis* extending much further from the inoculation zone as previously observed in other fungal-bacterial interaction.[14,23,76] In support to the mutualistic nature of the interaction, our findings highlight the functional significance of *B. velezensis* related to the fitness of AM fungi. The biofilm formed by *B. velezensis* may also serve as protective shield for its AM fungal host as illustrated by the toxicity of the secretome of *B. velezensis* dwelling in the hyphosphere toward potentially harmful microorganisms such as *T. harzianum* and *C. fungivorans*. Although we could not identify the full range of predicted BSMs, *B. velezensis* efficiently synthesizes multiple antimicrobial compounds in biofilm that do not only protect cells in biofilm against invasive organisms but that may also form a chemical barrier that contributes to safeguarding the AM fungi from microbial aggressors to compensate for the low natural potential of AM fungi to produce antibiotic weapons. We thus infer that AM fungi may selectively recruit members of the hyphosphere, such as *B. velezensis*, as protective agents, thereby expanding functionalities of the AM fungal-associated microbiome beyond their role in facilitating nutrient uptake.[14,18] This broadens the concept of the hyphosphere's impact on the selection of specific functional groups of bacteria in the hyphosphere of AM fungi to include antagonistic and biocontrol species such as *B. velezensis*.

In the other way, our results suggest that *Bacillus* may influence positively the fitness of various AM fungi in natural settings. However, given the observed differences in bacterial colonization rates, *B. velezensis* may preferentially promote the development of some species such as *R. irregularis* compared with others, thereby potentially influencing species competition. Further research is needed to fully investigate this hypothesis.

In a more applied perspective for biocontrol application, we also show that the interaction between *R. irregularis* and *B. velezensis* improves host resistance to *Botrytis cinerea* infection since combination of the two microorganisms confers higher systemic resistance compared with their application as single bioinoculants. On the one hand, this may be due to an enhanced mycorrhiza-induced resistance functionality of the AMF triggered by the bacterium, but nothing is known about the nature of fungal elicitors or effectors that could be boosted upon interaction. On the other hand, surfactin is the main compound produced by *B. velezensis* acting as elicitor of immune responses and systemic resistance in tomato and other Solanaceae[31,41,81,83] and we hypothesize that its translocation via the AM fungal ERM network may provide an optimal delivery at the root level in high amounts. A higher accumulation of surfactin at the root surface could also result from a higher population of *B. velezensis* since soil invasion by the bacterium is clearly facilitated in presence of the AMF. *Bacillus spp.* used as monospecies bioinoculants do not always meet expectations in the level and consistency of disease protection provided to crops, which is mainly due to poor or insufficient establishment of threshold populations in the soil environment under natural conditions

once introduced. Assessing whether such synergy between *R. irregularis* and *B. velezensis* may help to combat other diseases via ISR or direct antagonism requires further investigations, but the combination of the two microorganisms seems very promising as a new type of microbial consortium to be implemented in agricultural systems for sustainable crop production. A better understanding of the nature and dynamics of cross-kingdom interactions between these two microorganisms provides a way forward to engineering consortia with predictable compatibility and high biocontrol potential.

RESOURCE AVAILABILITY

Lead contact

Further information and requests for resources and reagents should be directed to and will be fulfilled by the lead contact, Marc Ongena (marc.ongena@uliege.be)

Materials availability

Bacterial strains used in this study are all available upon request. The AM fungi strains used in this study are all available in the catalog of BCCM/MUCL – GINCO, which can be accessed on their website: https://bccm.belspo.be/about-MUCL.

Data and code availability

- All datasets used to make the graphs presented in this work are publicly available at Mendeley Data: https://doi.org/10.17632/4sk92gx628.1.
- No specific codes have been developed for this study.
- Any additional information required to reanalyze the data reported in this paper is available from the lead contact upon request.

ACKNOWLEDGMENTS

This work was supported by the PDR research project (ID 40013634) from the F.R.S.-FNRS (National Fund for Scientific Research in Belgium), by the Microsoilsystem project funded by the Walloon Region (ID D31-1388SPW/DGO3), and by the EOS project (ID 30650620) from the FWO/F.R.S.-FNRS. A.A. and F.B. are recipients of an F.R.I.A. fellowship (F.R.S.-FNRS), and M.O. is Research Director at the F.R.S.-FNRS. We gratefully acknowledge Andrew Zickler and Francois Ferrais for technical help with the establishment of the experimental setup. We thank Jos Raaijmakers (Netherlands Institute for Ecology, Wageningen) and Monica Höfte (Ghent University) for their critical reading of the manuscript.

AUTHOR CONTRIBUTIONS

Conceptualization, A.A., S.D., and M.O.; methodology, A.A., F.B., S.S., and M.O.; investigation, A.A., L.-A.P., S.L., C.H., S.S., and A.A.-A.; resources, S.D. and M.O.; writing – original draft, A.A., S.D., and M.O.; writing – review & editing, A.A., M.C.-S., F.B., S.D., and M.O.; funding acquisition, S.D. and M.O.; supervision, S.D. and M.O.

DECLARATION OF INTERESTS

The authors declare no competing interests.

STAR★METHODS

Detailed methods are provided in the online version of this paper and include the following:

- KEY RESOURCES TABLE
- EXPERIMENTAL MODEL AND SUBJECT DETAILS
  - Biological materials
- METHOD DETAILS
  - Set up of experimental *in-vitro* system
  - Root and hyphae colonization by *B. velezensis in vitro*
  - Velocity of cytoplasmic flow
  - Succinate dehydrogenase (SDH) activity in hyphae
  - Impacts of BSMs on AM fungal hyphae
  - Bacterial CFU counting *in vitro*
  - *B. velezensis* biofilm formation along AM fungal hyphae of *R. irregularis*
  - *B. velezensis* metabolite production along AM fungal hyphae
  - *B. velezensis* metabolite production on *R. irregularis* exudates
  - *B. velezensis* metabolite production on carbohydrate compounds present in *R. irregularis* exudates
  - *B. velezensis* antimicrobial activity assays on hyphal exudates
  - Translocation of surfactin via the AM fungal network
  - Experimental design of greenhouse trial for *B. velezensis* common mycorrhizal network colonization
  - Effect of *B. velezensis* colonization on AM fungal population under greenhouse trial
  - ISR induction in tomato plants under greenhouse condition
  - Microbial root colonization under greenhouse trials
  - Quantification and statistical analysis

SUPPLEMENTAL INFORMATION

Supplemental information can be found online at https://doi.org/10.1016/j.cub.2024.09.019.

Received: December 1, 2023
Revised: July 26, 2024
Accepted: September 9, 2024
Published: October 7, 2024

REFERENCES

1. Wipf, D., Krajinski, F., van Tuinen, D., Recorbet, G., and Courty, P.E. (2019). Trading on the arbuscular mycorrhiza market: from arbuscules to common mycorrhizal networks. New Phytol. *223*, 1127–1142. https://doi.org/10.1111/nph.15775.
2. Brundrett, M.C., and Tedersoo, L. (2018). Evolutionary history of mycorrhizal symbioses and global host plant diversity. New Phytol. *220*, 1108–1115. https://doi.org/10.1111/nph.14976.
3. Parniske, M. (2008). Arbuscular mycorrhiza: the mother of plant root endosymbioses. Nat. Rev. Microbiol. *6*, 763–775. https://doi.org/10.1038/nrmicro1987.
4. Duhamel, M., Pel, R., Ooms, A., Bücking, H., Jansa, J., Ellers, J., Van Straalen, N.M., Wouda, T., Vandenkoornhuyse, P., and Kiers, E.T. (2013). Do fungivores trigger the transfer of protective metabolites from host plants to arbuscular mycorrhizal hyphae? Ecology *94*, 2019–2029. https://doi.org/10.1890/12-1943.1.
5. Johnson, D., and Gilbert, L. (2015). Interplant signalling through hyphal networks. New Phytol. *205*, 1448–1453. https://doi.org/10.1111/nph.13115.
6. Simard, S.W., Beiler, K.J., Bingham, M.A., Deslippe, J.R., Philip, L.J., and Teste, F.P. (2012). Mycorrhizal networks: Mechanisms, ecology and modelling. Fungal Biol. Rev. *26*, 39–60. https://doi.org/10.1016/j.fbr.2012.01.001.
7. Babikova, Z., Gilbert, L., Bruce, T.J.A., Birkett, M., Caulfield, J.C., Woodcock, C., Pickett, J.A., and Johnson, D. (2013). Underground signals carried through common mycelial networks warn neighbouring plants of aphid attack. Ecol. Lett. *16*, 835–843. https://doi.org/10.1111/ELE.12115.
8. Durant, E., Hoysted, G.A., Howard, N., Sait, S.M., Childs, D.Z., Johnson, D., and Field, K.J. (2023). Herbivore-driven disruption of arbuscular mycorrhizal carbon-for-nutrient exchange is ameliorated by neighboring plants. Curr. Biol. *33*, 2566–2573.e4. https://doi.org/10.1016/j.cub.2023.05.033.

9. Cameron, D.D., Neal, A.L., van Wees, S.C.M., and Ton, J. (2013). Mycorrhiza-induced resistance: more than the sum of its parts? Trends Plant Sci. *18*, 539–545. https://doi.org/10.1016/j.tplants.2013.06.004.

10. Jung, S.C., Martinez-Medina, A., Lopez-Raez, J.A., and Pozo, M.J. (2012). Mycorrhiza-Induced Resistance and Priming of Plant Defenses. J. Chem. Ecol. *38*, 651–664. https://doi.org/10.1007/s10886-012-0134-6.

11. Shi, J., Wang, X., and Wang, E. (2023). Mycorrhizal Symbiosis in Plant Growth and Stress Adaptation: From Genes to Ecosystems. Annu. Rev. Plant Biol. *74*, 569–607. https://doi.org/10.1146/annurev-arplant-061722-090342.

12. Scheublin, T.R., Sanders, I.R., Keel, C., and van der Meer, J.R. (2010). Characterisation of microbial communities colonising the hyphal surfaces of arbuscular mycorrhizal fungi. ISME J. *4*, 752–763. https://doi.org/10.1038/ismej.2010.5.

13. Luthfiana, N., Inamura, N., Tantriani, Sato, T., Saito, K., Oikawa, A., Chen, W., and Tawaraya, K. (2021). Metabolite profiling of the hyphal exudates of Rhizophagus clarus and Rhizophagus irregularis under phosphorus deficiency. Mycorrhiza *31*, 403–412. https://doi.org/10.1007/s00572-020-01016-z.

14. Zhang, L., Zhou, J., George, T.S., Limpens, E., and Feng, G. (2022). Arbuscular mycorrhizal fungi conducting the hyphosphere bacterial orchestra. Trends Plant Sci. *27*, 402–411. https://doi.org/10.1016/j.tplants.2021.10.008.

15. Toljander, J.F., Lindahl, B.D., Paul, L.R., Elfstrand, M., and Finlay, R.D. (2007). Influence of arbuscular mycorrhizal mycelial exudates on soil bacterial growth and community structure. FEMS Microbiol. Ecol. *61*, 295–304. https://doi.org/10.1111/j.1574-6941.2007.00337.x.

16. Emmett, B.D., Lévesque-Tremblay, V., and Harrison, M.J. (2021). Conserved and reproducible bacterial communities associate with extraradical hyphae of arbuscular mycorrhizal fungi. ISME J. *15*, 2276–2288. https://doi.org/10.1038/s41396-021-00920-2.

17. Basiru, S., Ait Si Mhand, K., and Hijri, M. (2023). Disentangling arbuscular mycorrhizal fungi and bacteria at the soil-root interface. Mycorrhiza *33*, 119–137. https://doi.org/10.1007/s00572-023-01107-7.

18. Faghihinia, M., Jansa, J., Halverson, L.J., and Staddon, P.L. (2023). Hyphosphere microbiome of arbuscular mycorrhizal fungi: a realm of unknowns. Biol. Fertil. Soils *59*, 17–34. https://doi.org/10.1007/s00374-022-01683-4.

19. Duan, S., Feng, G., Limpens, E., Bonfante, P., Xie, X., and Zhang, L. (2024). Cross-kingdom nutrient exchange in the plant–arbuscular mycorrhizal fungus–bacterium continuum.. Published online July 16, 2024. Nat. Rev. Microbiol. *xxx*, xxx. https://doi.org/10.1038/s41579-024-01073-7.

20. Jin, Z., Jiang, F., Wang, L., Declerck, S., Feng, G., and Zhang, L. (2024). Arbuscular mycorrhizal fungi and Streptomyces: brothers in arms to shape the structure and function of the hyphosphere microbiome in the early stage of interaction. Microbiome *12*, 1. https://doi.org/10.1186/s40168-023-01727-3.

21. Zhang, L., Feng, G., and Declerck, S. (2018). Signal beyond nutrient, fructose, exuded by an arbuscular mycorrhizal fungus triggers phytate mineralization by a phosphate solubilizing bacterium. ISME J. *12*, 2339–2351. https://doi.org/10.1038/s41396-018-0171-4.

22. Li, X., Zhao, R., Li, D., Wang, G., Bei, S., Ju, X., An, R., Li, L., Kuyper, T.W., Christie, P., et al. (2023). Mycorrhiza-mediated recruitment of complete denitrifying *Pseudomonas* reduces N2O emissions from soil. Microbiome *11*, 45. https://doi.org/10.1186/s40168-023-01466-5.

23. Jiang, F., Zhang, L., Zhou, J., George, T.S., and Feng, G. (2021). Arbuscular mycorrhizal fungi enhance mineralisation of organic phosphorus by carrying bacteria along their extraradical hyphae. New Phytol. *230*, 304–315. https://doi.org/10.1111/nph.17081.

24. St-Arnaud, M., Hamel, C., Vimard, B., Caron, M., and Fortin, J.A. (1996). Enhanced hyphal growth and spore production of the arbuscular mycorrhizal fungus *Glomus intraradices* in an in vitro system in the absence of host roots. Mycol. Res. *100*, 328–332. https://doi.org/10.1016/S0953-7562(96)80164-X.

25. Cranenbrouck, S., Voets, L., Bivort, C., Renard, L., Strullu, D.-G., and Declerck, S. (2005). Methodologies for in Vitro Cultivation of Arbuscular Mycorrhizal Fungi with Root Organs. In In Vitro Culture of Mycorrhizas (Springer), pp. 341–375. https://doi.org/10.1007/3-540-27331-X_18.

26. Whiteside, M.D., Werner, G.D.A., Caldas, V.E.A., van't Padje, A., Dupin, S.E., Elbers, B., Bakker, M., Wyatt, G.A.K., Klein, M., Hink, M.A., et al. (2019). Mycorrhizal Fungi Respond to Resource Inequality by Moving Phosphorus from Rich to Poor Patches across Networks. Curr. Biol. *29*, 2043–2050.e8. https://doi.org/10.1016/J.CUB.2019.04.061.

27. Wang, F., Zhang, L., Zhou, J., Rengel, Z., George, T.S., and Feng, G. (2022). Exploring the secrets of hyphosphere of arbuscular mycorrhizal fungi: processes and ecological functions. Plant Soil *481*, 1–22. https://doi.org/10.1007/s11104-022-05621-z.

28. Alaux, P.-L., Naveau, F., Declerck, S., and Cranenbrouck, S. (2020). Common Mycorrhizal Network Induced JA/ET Genes Expression in Healthy Potato Plants Connected to Potato Plants Infected by *Phytophthora infestans*. Front. Plant Sci. *11*, 602. https://doi.org/10.3389/fpls.2020.00602.

29. Andrić, S., Meyer, T., and Ongena, M. (2020). *Bacillus* Responses to Plant-Associated Fungal and Bacterial Communities. Front. Microbiol. *11*, 1350. https://doi.org/10.3389/fmicb.2020.01350.

30. Andrić, S., Rigolet, A., Argüelles Arias, A., Steels, S., Hoff, G., Balleux, G., Ongena, L., Höfte, M., Meyer, T., and Ongena, M. (2023). Plant-associated *Bacillus* mobilizes its secondary metabolites upon perception of the siderophore pyochelin produced by a *Pseudomonas* competitor. ISME J. *17*, 263–275. https://doi.org/10.1038/s41396-022-01337-1.

31. Hoff, G., Arguelles Arias, A., Boubsi, F., Pršić, J., Meyer, T., Ibrahim, H.M.M., Steels, S., Luzuriaga, P., Legras, A., Franzil, L., et al. (2021). Surfactin Stimulated by Pectin Molecular Patterns and Root Exudates Acts as a Key Driver of the *Bacillus*-Plant Mutualistic Interaction. mBio *12*, e0177421. https://doi.org/10.1128/mBio.01774-21.

32. Boubsi, F., Hoff, G., Arguelles Arias, A., Steels, S., Andrić, S., Anckaert, A., Roulard, R., Rigolet, A., van Wuytswinkel, O., and Ongena, M. (2023). Pectic homogalacturonan sensed by *Bacillus* acts as host associated cue to promote establishment and persistence in the rhizosphere. iScience *26*, 107925. https://doi.org/10.1016/j.isci.2023.107925.

33. Loján, P., Demortier, M., Velivelli, S.L.S., Pfeiffer, S., Suárez, J.P., de Vos, P., Prestwich, B.D., Sessitsch, A., and Declerck, S. (2017). Impact of plant growth-promoting rhizobacteria on root colonization potential and life cycle of *Rhizophagus irregularis* following co-entrapment into alginate beads. J. Appl. Microbiol. *122*, 429–440. https://doi.org/10.1111/jam.13355.

34. Alaux, P.-L., César, V., Naveau, F., Cranenbrouck, S., and Declerck, S. (2018). Impact of *Rhizophagus irregularis* MUCL 41833 on disease symptoms caused by *Phytophthora infestans* in potato grown under field conditions. Crop Prot. *107*, 26–33. https://doi.org/10.1016/j.cropro.2018.01.003.

35. Gbongue, L.-R., Lalaymia, I., Zeze, A., Delvaux, B., and Declerck, S. (2018). Increased Silicon Acquisition in Bananas Colonized by Rhizophagus irregularis MUCL 41833 Reduces the Incidence of *Pseudocercospora fijiensis*. Front. Plant Sci. *9*, 1977. https://doi.org/10.3389/fpls.2018.01977.

36. Arnaouteli, S., Bamford, N.C., Stanley-Wall, N.R., and Kovács, Á.T. (2021). *Bacillus subtilis* biofilm formation and social interactions. Nat. Rev. Microbiol. *19*, 600–614. https://doi.org/10.1038/s41579-021-00540-9.

37. Allard-Massicotte, R., Tessier, L., Lécuyer, F., Lakshmanan, V., Lucier, J.-F., Garneau, D., Caudwell, L., Vlamakis, H., Bais, H.P., and Beauregard, P.B. (2016). *Bacillus subtilis* Early Colonization of Arabidopsis thaliana Roots Involves Multiple Chemotaxis Receptors. mBio *7*, e01664-16. https://doi.org/10.1128/mBio.01664-16.

38. Bago, B., Azcón-aguilar, C., Goulet, A., and Piché, Y. (1998). Branched absorbing structures (BAS): a feature of the extraradical mycelium of symbiotic arbuscular mycorrhizal fungi. New Phytol. *139*, 375–388. https://doi.org/10.1046/j.1469-8137.1998.00199.x.

39. Karygianni, L., Ren, Z., Koo, H., and Thurnheer, T. (2020). Biofilm Matrixome: Extracellular Components in Structured Microbial Communities. Trends Microbiol. *28*, 668–681. https://doi.org/10.1016/j.tim.2020.03.016.

40. Massalha, H., Korenblum, E., Malitsky, S., Shapiro, O.H., and Aharoni, A. (2017). Live imaging of root–bacteria interactions in a microfluidics setup. Proc. Natl. Acad. Sci. USA *114*, 4549–4554. https://doi.org/10.1073/pnas.1618584114.

41. Stoll, A., Salvatierra-Martínez, R., González, M., and Araya, M. (2021). The Role of Surfactin Production by Bacillus velezensis on Colonization, Biofilm Formation on Tomato Root and Leaf Surfaces and Subsequent Protection (ISR) against *Botrytis cinerea*. Microorganisms *9*, 2251. https://doi.org/10.3390/microorganisms9112251.

42. Luo, C., Zhou, H., Zou, J., Wang, X., Zhang, R., Xiang, Y., and Chen, Z. (2015). Bacillomycin L and surfactin contribute synergistically to the phenotypic features of *Bacillus subtilis* 916 and the biocontrol of rice sheath blight induced by *Rhizoctonia solani*. Appl. Microbiol. Biotechnol. *99*, 1897–1910. https://doi.org/10.1007/s00253-014-6195-4.

43. Cao, Y., Pi, H., Chandrangsu, P., Li, Y., Wang, Y., Zhou, H., Xiong, H., Helmann, J.D., and Cai, Y. (2018). Antagonism of Two Plant-Growth Promoting Bacillus velezensis Isolates Against *Ralstonia solanacearum* and *Fusarium oxysporum*. Sci. Rep. *8*, 4360. https://doi.org/10.1038/s41598-018-22782-z.

44. Ghelardi, E., Salvetti, S., Ceragioli, M., Gueye, S.A., Celandroni, F., and Senesi, S. (2012). Contribution of Surfactin and SwrA to Flagellin Expression, Swimming, and Surface Motility in *Bacillus subtilis*. Appl. Environ. Microbiol. *78*, 6540–6544. https://doi.org/10.1128/AEM.01341-12.

45. Al-Ali, A., Deravel, J., Krier, F., Béchet, M., Ongena, M., and Jacques, P. (2018). Biofilm formation is determinant in tomato rhizosphere colonization by Bacillus velezensis FZB42. Environ. Sci. Pollut. Res. Int. *25*, 29910–29920. https://doi.org/10.1007/s11356-017-0469-1.

46. Schaffer, G.F., and Peterson, R.L. (1993). Modifications to clearing methods used in combination with vital staining of roots colonized with vesicular-arbuscular mycorrhizal fungi. Mycorrhiza *4*, 29–35. https://doi.org/10.1007/BF00203248.

47. Bago, B., Zipfel, W., Williams, R.M., Jun, J., Arreola, R., Lammers, P.J., Pfeffer, P.E., and Shachar-Hill, Y. (2002). Translocation and Utilization of Fungal Storage Lipid in the Arbuscular Mycorrhizal Symbiosis. Plant Physiol. *128*, 108–124. https://doi.org/10.1104/pp.010466.

48. Hammer, E.C., Arellano-Caicedo, C., Mafla-Endara, P.M., Kiers, E.T., Shimizu, T., Ohlsson, P., and Aleklett, K. (2024). Hyphal exploration strategies and habitat modification of an arbuscular mycorrhizal fungus in microengineered soil chips. Fungal Ecol. *67*, 101302. https://doi.org/10.1016/J.FUNECO.2023.101302.

49. Traxler, M.F., and Kolter, R. (2015). Natural products in soil microbe interactions and evolution. Nat. Prod. Rep. *32*, 956–970. https://doi.org/10.1039/C5NP00013K.

50. Ongena, M., and Jacques, P. (2008). *Bacillus* lipopeptides: versatile weapons for plant disease biocontrol. Trends Microbiol. *16*, 115–125. https://doi.org/10.1016/j.tim.2007.12.009.

51. Anckaert, A., Arias, A.A., Hoff, G., Calonne-Salmon, M., Declerck, S., and Ongena, M. (2021). The use of *Bacillus* spp. as bacterial biocontrol agents to control plant diseases. In Microbial Bioprotectants for Plant Disease Management, W. Ravensberg, and J. Köhl, eds. (Burleigh Dodds Science Publishing), pp. 247–300. https://doi.org/10.19103/AS.2021.0093.10.

52. Mantil, E., Buznytska, I., Daly, G., Ianoul, A., and Avis, T.J. (2019). Role of Lipid Composition in the Interaction and Activity of the Antimicrobial Compound Fengycin with Complex Membrane Models. J. Membr. Biol. *252*, 627–638. https://doi.org/10.1007/s00232-019-00100-6.

53. Balleza, D., Alessandrini, A., and Beltrán García, M.J. (2019). Role of Lipid Composition, Physicochemical Interactions, and Membrane Mechanics in the Molecular Actions of Microbial Cyclic Lipopeptides. J. Membr. Biol. *252*, 131–157. https://doi.org/10.1007/s00232-019-00067-4.

54. Nasir, M.N., Thawani, A., Kouzayha, A., and Besson, F. (2010). Interactions of the natural antimicrobial mycosubtilin with phospholipid membrane models. Colloids Surf. B Biointerfaces *78*, 17–23. https://doi.org/10.1016/j.colsurfb.2010.01.034.

55. Nihorimbere, V., Cawoy, H., Seyer, A., Brunelle, A., Thonart, P., and Ongena, M. (2012). Impact of rhizosphere factors on cyclic lipopeptide signature from the plant beneficial strain *Bacillus amyloliquefaciens* S499. FEMS Microbiol. Ecol. *79*, 176–191. https://doi.org/10.1111/j.1574-6941.2011.01208.x.

56. Medeot, D.B., Bertorello-Cuenca, M., Liaudat, J.P., Alvarez, F., Flores-Cáceres, M.L., and Jofré, E. (2017). Improvement of biomass and cyclic lipopeptides production in *Bacillus amyloliquefaciens* MEP218 by modifying carbon and nitrogen sources and ratios of the culture media. Biol. Control *115*, 119–128. https://doi.org/10.1016/j.biocontrol.2017.10.002.

57. Lu, H., Qian, S., Muhammad, U., Jiang, X., Han, J., and Lu, Z. (2016). Effect of fructose on promoting fengycin biosynthesis in *Bacillus amyloliquefaciens* fmb-60. J. Appl. Microbiol. *121*, 1653–1664. https://doi.org/10.1111/jam.13291.

58. Purin, S., and Rillig, M.C. (2008). Parasitism of arbuscular mycorrhizal fungi: reviewing the evidence. FEMS Microbiol. Lett. *279*, 8–14. https://doi.org/10.1111/j.1574-6968.2007.01007.x.

59. De Jaeger, N., Declerck, S., and De La Providencia, I.E. (2010). Mycoparasitism of arbuscular mycorrhizal fungi: a pathway for the entry of saprotrophic fungi into roots. FEMS Microbiol. Ecol. *73*, 312–322. https://doi.org/10.1111/J.1574-6941.2010.00903.X.

60. Xie, J., Sun, X., Xia, Y., Tao, L., Tan, T., Zhang, N., Xun, W., Zhang, R., Kovács, Á.T., Xu, Z., et al. (2024). Bridging the Gap: biofilm-mediated establishment of Bacillus velezensis on Trichoderma guizhouense mycelia. Preprint at bioRxiv *xxx*, xxx. https://doi.org/10.1101/2024.06.06.597722.

61. Fifani, B., Steels, S., Helmus, C., Delacuvellerie, A., Deracinois, B., Phalip, V., Delvigne, F., and Jacques, P. (2022). Coculture of *Trichoderma harzianum* and *Bacillus velezensis* Based on Metabolic Cross-Feeding Modulates Lipopeptide Production. Microorganisms *10*, 1059. https://doi.org/10.3390/microorganisms10051059.

62. Williamson, B., Tudzynski, B., Tudzynski, P., and Van Kan, J.A.L. (2007). *Botrytis cinerea*: the cause of grey mould disease. Mol. Plant Pathol. *8*, 561–580. https://doi.org/10.1111/j.1364-3703.2007.00417.x.

63. Dean, R., Van Kan, J.A.L., Pretorius, Z.A., Hammond-Kosack, K.E., Di Pietro, A., Spanu, P.D., Rudd, J.J., Dickman, M., Kahmann, R., Ellis, J., et al. (2012). The Top 10 fungal pathogens in molecular plant pathology. Mol. Plant Pathol. *13*, 414–430. https://doi.org/10.1111/j.1364-3703.2011.00783.x.

64. Scherlach, K., and Hertweck, C. (2020). Chemical Mediators at the Bacterial-Fungal Interface. Annu. Rev. Microbiol. *74*, 267–290. https://doi.org/10.1146/ANNUREV-MICRO-012420-081224.

65. Ali, S., Hameed, S., Shahid, M., Iqbal, M., Lazarovits, G., and Imran, A. (2020). Functional characterization of potential PGPR exhibiting broad-spectrum antifungal activity. Microbiol. Res. *232*, 126389. https://doi.org/10.1016/J.MICRES.2019.126389.

66. Deveau, A., Bonito, G., Uehling, J., Paoletti, M., Becker, M., Bindschedler, S., Hacquard, S., Hervé, V., Labbé, J., Lastovetsky, O.A., et al. (2018). Bacterial-fungal interactions: ecology, mechanisms and challenges. FEMS Microbiol. Rev. *42*, 335–352. https://doi.org/10.1093/femsre/fuy008.

67. Abeysinghe, G., Kuchira, M., Kudo, G., Masuo, S., Ninomiya, A., Takahashi, K., Utada, A.S., Hagiwara, D., Nomura, N., Takaya, N., et al. (2020). Fungal mycelia and bacterial thiamine establish a mutualistic growth mechanism. Life Sci. Alliance *3*, e202000878. https://doi.org/10.26508/lsa.202000878.

68. Arrebola, E., Jacobs, R., and Korsten, L. (2010). Iturin A is the principal inhibitor in the biocontrol activity of *Bacillus amyloliquefaciens* PPCB004

against postharvest fungal pathogens. J. Appl. Microbiol. *108*, 386–395. https://doi.org/10.1111/j.1365-2672.2009.04438.x.

69. Jiang, C.-H., Liao, M.-J., Wang, H.-K., Zheng, M.-Z., Xu, J.-J., and Guo, J.-H. (2018). *Bacillus velezensis*, a potential and efficient biocontrol agent in control of pepper gray mold caused by *Botrytis cinerea*. Biol. Control *126*, 147–157. https://doi.org/10.1016/j.biocontrol.2018.07.017.
70. Calvo, H., Mendiara, I., Arias, E., Blanco, D., and Venturini, M.E. (2019). The role of iturin A from *B. amyloliquefaciens* BUZ-14 in the inhibition of the most common postharvest fruit rots. Food Microbiol. *82*, 62–69. https://doi.org/10.1016/j.fm.2019.01.010.
71. Weete, J.D., Abril, M., and Blackwell, M. (2010). Phylogenetic Distribution of Fungal Sterols. PLoS One *5*, e10899. https://doi.org/10.1371/journal.pone.0010899.
72. Wewer, V., Brands, M., and Dörmann, P. (2014). Fatty acid synthesis and lipid metabolism in the obligate biotrophic fungus *Rhizophagus irregularis* during mycorrhization of *Lotus japonicus*. Plant J. *79*, 398–412. https://doi.org/10.1111/tpj.12566.
73. Kameoka, H., and Gutjahr, C. (2022). Functions of Lipids in Development and Reproduction of Arbuscular Mycorrhizal Fungi. Plant Cell Physiol. *63*, 1356–1365. https://doi.org/10.1093/pcp/pcac113.
74. Ongena, M., Jacques, P., Touré, Y., Destain, J., Jabrane, A., and Thonart, P. (2005). Involvement of fengycin-type lipopeptides in the multifaceted biocontrol potential of *Bacillus subtilis*. Appl. Microbiol. Biotechnol. *69*, 29–38. https://doi.org/10.1007/s00253-005-1940-3.
75. Fan, H., Ru, J., Zhang, Y., Wang, Q., and Li, Y. (2017). Fengycin produced by *Bacillus subtilis* 9407 plays a major role in the biocontrol of apple ring rot disease. Microbiol. Res. *199*, 89–97. https://doi.org/10.1016/j.micres.2017.03.004.
76. Zhang, L., Xu, M., Liu, Y., Zhang, F., Hodge, A., and Feng, G. (2016). Carbon and phosphorus exchange may enable cooperation between an arbuscular mycorrhizal fungus and a phosphate-solubilizing bacterium. New Phytol. *210*, 1022–1032. https://doi.org/10.1111/nph.13838.
77. Kobayashi, K. (2015). Plant methyl salicylate induces defense responses in the rhizobacterium *Bacillus subtilis*. Environ. Microbiol. *17*, 1365–1376. https://doi.org/10.1111/1462-2920.12613.
78. Park, S.-W., Kaimoyo, E., Kumar, D., Mosher, S., and Klessig, D.F. (2007). Methyl Salicylate Is a Critical Mobile Signal for Plant Systemic Acquired Resistance. Science *318*, 113–116. https://doi.org/10.1126/science.1147113.
79. Bais, H.P., Fall, R., and Vivanco, J.M. (2004). Biocontrol of *Bacillus subtilis* against Infection of Arabidopsis Roots by Pseudomonas syringae Is Facilitated by Biofilm Formation and Surfactin Production. Plant Physiol. *134*, 307–319. https://doi.org/10.1104/pp.103.028712.
80. Aleti, G., Lehner, S., Bacher, M., Compant, S., Nikolic, B., Plesko, M., Schuhmacher, R., Sessitsch, A., and Brader, G. (2016). Surfactin variants mediate species-specific biofilm formation and root colonization in *Bacillus*. Environ. Microbiol. *18*, 2634–2645. https://doi.org/10.1111/1462-2920.13405.
81. Henry, G., Deleu, M., Jourdan, E., Thonart, P., and Ongena, M. (2011). The bacterial lipopeptide surfactin targets the lipid fraction of the plant plasma membrane to trigger immune-related defence responses. Cell. Microbiol. *13*, 1824–1837. https://doi.org/10.1111/j.1462-5822.2011.01664.x.
82. Deleu, M., Lorent, J., Lins, L., Brasseur, R., Braun, N., El Kirat, K., Nylander, T., Dufrêne, Y.F., and Mingeot-Leclercq, M.P. (2013). Effects of surfactin on membrane models displaying lipid phase separation. Biochim. Biophys. Acta *1828*, 801–815. https://doi.org/10.1016/j.bbamem.2012.11.007.
83. Ongena, M., Jourdan, E., Adam, A., Paquot, M., Brans, A., Joris, B., Arpigny, J.-L., and Thonart, P. (2007). Surfactin and fengycin lipopeptides of *Bacillus subtilis* as elicitors of induced systemic resistance in plants. Environ. Microbiol. *9*, 1084–1090. https://doi.org/10.1111/j.1462-2920.2006.01202.x.
84. Raaijmakers, J.M., de Bruijn, I., Nybroe, O., and Ongena, M. (2010). Natural functions of lipopeptides from *Bacillus* and *Pseudomonas*: more than surfactants and antibiotics. FEMS Microbiol. Rev. *34*, 1037–1062. https://doi.org/10.1111/J.1574-6976.2010.00221.X.
85. Oni, F.E., Esmaeel, Q., Onyeka, J.T., Adeleke, R., Jacquard, C., Clement, C., Gross, H., Ait Barka, E.A., and Höfte, M. (2022). Pseudomonas Lipopeptide-Mediated Biocontrol: Chemotaxonomy and Biological Activity. Molecules *27*, 372. https://doi.org/10.3390/MOLECULES27020372.
86. Worrich, A., Stryhanyuk, H., Musat, N., König, S., Banitz, T., Centler, F., Frank, K., Thullner, M., Harms, H., Richnow, H.H., et al. (2017). Mycelium-mediated transfer of water and nutrients stimulates bacterial activity in dry and oligotrophic environments. Nat. Commun. *8*, 15472. https://doi.org/10.1038/ncomms15472.
87. Miquel Guennoc, C.M., Rose, C., Labbé, J., and Deveau, A. (2018). Bacterial biofilm formation on the hyphae of ectomycorrhizal fungi: A widespread ability under controls? FEMS Microbiol. Ecol. *94*, 1–14. https://doi.org/10.1093/femsec/fiy093.
88. Kjeldgaard, B., Listian, S.A., Ramaswamhi, V., Richter, A., Kiesewalter, H.T., and Kovács, Á.T. (2019). Fungal hyphae colonization by Bacillus subtilis relies on biofilm matrix components. Biofilm *1*, 100007. https://doi.org/10.1016/j.bioflm.2019.100007.
89. Andrade, G., Mihara, K.L., Linderman, R.G., and Bethlenfalvay, G.J. (1997). Bacteria from rhizosphere and hyphosphere soils of different arbuscular-mycorrhizal fungi. Plant Soil *192*, 71–79. https://doi.org/10.1023/A:1004249629643.
90. Battini, F., Cristani, C., Giovannetti, M., and Agnolucci, M. (2016). Multifunctionality and diversity of culturable bacterial communities strictly associated with spores of the plant beneficial symbiont *Rhizophagus intraradices*. Microbiol. Res. *183*, 68–79. https://doi.org/10.1016/j.micres.2015.11.012.
91. Xavier, L.J.C., and Germida, J.J. (2003). Bacteria associated with *Glomus clarum* spores influence mycorrhizal activity. Soil Biol. Biochem. *35*, 471–478. https://doi.org/10.1016/S0038-0717(03)00003-8.
92. Lecomte, J., St-Arnaud, M., and Hijri, M. (2011). Isolation and identification of soil bacteria growing at the expense of arbuscular mycorrhizal fungi. FEMS Microbiol. Lett. *317*, 43–51. https://doi.org/10.1111/J.1574-6968.2011.02209.X.
93. Agnolucci, M., Battini, F., Cristani, C., and Giovannetti, M. (2015). Diverse bacterial communities are recruited on spores of different arbuscular mycorrhizal fungal isolates. Biol. Fertil. Soils *51*, 379–389. https://doi.org/10.1007/s00374-014-0989-5.
94. Flemming, H.-C., Wingender, J., Szewzyk, U., Steinberg, P., Rice, S.A., and Kjelleberg, S. (2016). Biofilms: an emergent form of bacterial life. Nat. Rev. Microbiol. *14*, 563–575. https://doi.org/10.1038/nrmicro.2016.94.
95. Molina-Santiago, C., Pearson, J.R., Navarro, Y., Berlanga-Clavero, M.V., Caraballo-Rodriguez, A.M., Petras, D., García-Martín, M.L., Lamon, G., Haberstein, B., Cazorla, F.M., et al. (2019). The extracellular matrix protects *Bacillus subtilis* colonies from *Pseudomonas* invasion and modulates plant co-colonization. Nat. Commun. *10*, 1919. https://doi.org/10.1038/s41467-019-09944-x.
96. Kohlmeier, S., Smits, T.H.M., Ford, R.M., Keel, C., Harms, H., and Wick, L.Y. (2005). Taking the fungal highway: Mobilization of pollutant-degrading bacteria by fungi. Environ. Sci. Technol. *39*, 4640–4646. https://doi.org/10.1021/es047979z.
97. Schindelin, J., Arganda-Carreras, I., Frise, E., Kaynig, V., Longair, M., Pietzsch, T., Preibisch, S., Rueden, C., Saalfeld, S., Schmid, B., et al. (2012). Fiji: an open-source platform for biological-image analysis. Nat. Methods *9*, 676–682. https://doi.org/10.1038/nmeth.2019.
98. Tinevez, J.Y., Perry, N., Schindelin, J., Hoopes, G.M., Reynolds, G.D., Laplantine, E., Bednarek, S.Y., Shorte, S.L., and Eliceiri, K.W. (2017). TrackMate: An open and extensible platform for single-particle tracking. Methods *115*, 80–90. https://doi.org/10.1016/j.ymeth.2016.09.016.

99. Declerck, S., Strullu, D.G., and Plenchette, C. (1998). Monoxenic culture of the intraradical forms of *Glomus* sp. isolated from a tropical ecosystem: a proposed methodology for germplasm collection. Mycologia *90*, 579–585. https://doi.org/10.1080/00275514.1998.12026946.

100. Jarmer, H., Berka, R., Knudsen, S., and Saxild, H.H. (2002). Transcriptome analysis documents induced competence of *Bacillus subtilis* during nitrogen limiting conditions. FEMS Microbiol. Lett. *206*, 197–200. https://doi.org/10.1111/j.1574-6968.2002.tb11009.x.

101. Calonne, M., Fontaine, J., Tisserant, B., Dupré de Boulois, H., Grandmougin-Ferjani, A., Declerck, S., and Lounès-Hadj Sahraoui, A. (2014). Polyaromatic hydrocarbons impair phosphorus transport by the arbuscular mycorrhizal fungus *Rhizophagus irregularis*. Chemosphere *104*, 97–104. https://doi.org/10.1016/J.CHEMOSPHERE.2013.10.070.

102. Garcés-Ruiz, M., Calonne-Salmon, M., Plouznikoff, K., Misson, C., Navarrete-Mier, M., Cranenbrouck, S., and Declerck, S. (2017). Dynamics of short-term phosphorus uptake by intact mycorrhizal and non-mycorrhizal maize plants grown in a circulatory semi-hydroponic cultivation system. Front. Plant Sci. *8*, 1471. https://doi.org/10.3389/fpls.2017.01471.

STAR★METHODS

KEY RESOURCES TABLE

REAGENT or RESOURCE	SOURCE	IDENTIFIER
Bacterial and virus strains		
Bacillus velezensis GA1 and mutants (see Table S1)		N/A
Collimonas fungivorans LMG 21973	BCCM/LMG	Cat# LMG21973
Chemicals, peptides, and recombinant proteins		
MOPS	SIGMA-ALDRICH	Cat# M1254
Phytagel™	SIGMA-ALDRICH	Cat# P8169
Agarose	NIPPON Genetics Europe	Cat# AG02
Propidium Iodide	ThermoFisher Scientific	Cat# P1304MP
DNAzol™ Reagent	ThermoFisher Scientific	Cat# 10503027
Nitro Blue Tetrazolium (NBT)	SIGMA-ALDRICH	Cat# N6639
Chloramphenicol	AppliChem	Cat# A1806
Phleomycin	InvivoGen	Cat# ant-ph-1
Surfactin	Prof. Ongena Marc, Microbial Processes and Interactions Laboratory, Uliège, Belgium	N/A
Fengycin	Prof. Ongena Marc, Microbial Processes and Interactions Laboratory, Uliège, Belgium	N/A
Iturin	Prof. Ongena Marc, Microbial Processes and Interactions Laboratory, Uliège, Belgium	N/A
Tris-HCl	Sigma	Cat# T3253
Tween20	Sigma	Cat# P9416
Critical commercial assays		
NucleoSpin RNA Kit	Macherey Nagel	Cat# 740955.250
Luna® Universal One-Step RT-qPCR Kit	New England Biolabs	Cat# E3005L
QuantiFluor dsDNA system	Promega	Cat# E2670
GenEluteTM Soil DNA Isolation kit	SIGMA-ALDRICH	Cat# DNB100
Experimental models: Organisms/strains		
Solanum lycopersicum cv Ailsa Criag and cv MoneyMakers	EnGraineToi	N/A
Botrytis cinerea MUCL 43839	BCCM/MUCL	Cat# MUCL43839
Solanum tuberosum L. var. Bintje	Station de Haute Belgique	N/A
Trichoderma harzianum Rifai MUCL 29707	BCCM/MUCL	Cat# MUCL29707
Rhizophagus irregularis (Błaszk,Wubet, Renker, and Buscot) C. Walker and A. Schüßler as (“irregulare”) MUCL 41833	BCCM/MUCL - GINCO	Cat# MUCL41833
Rhizophagus clarus (T.H. Nicolson & N.C. Schenck) C. Walker & A. Schüßler MUCL 46238	BCCM/MUCL - GINCO	Cat# MUCL46238
Rhizophagus intraradices (N.C. Schenck & G.S. Sm.) C. Walker & Schuessler MUCL 49410	BCCM/MUCL – GINCO	Cat# MUCL 49410
Rhizophagus aggregatus (N.C. Schenck & G.S. Sm.) C. Walker MUCL 49408	BCCM/MUCL – GINCO	Cat# MUCL 49408
Oligonucleotides		
Primers (see Table S2)		N/A

(*Continued on next page*)

Continued

REAGENT or RESOURCE	SOURCE	IDENTIFIER
Software and algorithms		
Fiji (ImageJ)	Schindelin et al.[97]	RRID: SCR_002285
MassHunter v10.0	Agilent	https://www.agilent.com/en/product/software-informatics/mass-spectrometry-software; RRID: SCR_015742
NIS-Element AR software	Nikon	https://www.microscope.healthcare.nikon.com/products/software/nis-elements/nis-elements-advanced-research
GraphPad Prism 9	GraphPad Software	RRID: SCR_002798
TrackMate	Tinevez et al.[98]	N/A
Other		
SPARK multiplate reader	Tecan	https://lifesciences.tecan.com/multimode-plate-reader
NanoDrop 2000	ThermoFisher Scientific	Cat# ND-2000; RRID: SCR_018042
StepOne™ Real-Time PCR system	ThermoFisher Scientific	Cat# 4376357; RRID: SCR_015805
UHPLC Agilent 1290 Infinity II	Agilent	https://www.agilent.com/en/product/liquid-chromatography/hplc-systems/analytical-hplc-systems/1290-infinity-ii-lc-system; RRID: SCR_019378
Acquity UPLC BEH C18 column (2.1 x 50mm x 1.7μm)	Waters	Cat# 186002350
6530 Q-TOF mass spectrometer	Agilent	Cat# G6530AA; RRID: SCR_019423
Nikon Ti2-E inverted microscope	Nikon	https://www.microscope.healthcare.nikon.com/products/inverted-microscopes/eclipse-ti2-series; RRID: SCR_021242
Petri dishes- 90mm, 3 compartments, vents	VWR	Cat# KART363
Petri dishes- 90mm, 2 compartments, vents	Greiner bio-one	Cat# 635161

EXPERIMENTAL MODEL AND SUBJECT DETAILS

Biological materials

Rhizophagus irregularis (Błaszk,Wubet, Renker, and Buscot) C. Walker and A. Schüßler as (“irregulare”) MUCL 41833, *Rhizophagus clarus* (T.H. Nicolson & N.C. Schenck) C. Walker & A. Schüßler MUCL 46238, *Rhizophagus aggregatus* (N.C. Schenck & G.S. Sm.) C. Walker MUCL 49408 *and Rhizophagus intraradices* (N.C. Schenck & G.S. Sm.) C. Walker & Schuessler MUCL 49410 were obtained from the Glomeromycota *in vitro* collection (GINCO). AM fungi were proliferated *in vitro* on Ri T-DNA transformed roots of carrot (*Daucus carota* L.) clone DC2 in bi-compartmented Petri plates (90 × 15 mm) containing the Modified Strullu-Romand (MSR) medium.[99] The Petri plates were incubated in the dark at 27 °C until sufficient spores were produced.

Bacillus velezensis GA1 and its mutants are listed in Table S1. The construction of knockout mutant strains of *B. velezensis* GA1 involved gene replacement through homologous recombination as previously described by Hoff et al.[31] The procedure involved PCR amplification of the 1 kb upstream region of the target gene, the antibiotic marker (chloramphenicol, kanamycin and/or phleomycin cassette), and the 1kb downstream region of the target gene, using appropriate primers. The primers used for this study have been previously described by Andric et al.[30] and listed in Table S2.To introduce the recombinant cassette into GA1, a slightly modified protocol developed by Jarmer et al.[100] was employed by inducing natural competence through nitrogen depletion. Initially, a colony of *B. velezensis* was inoculated on lysogeny broth (LB) medium (10 g $l^{-(}$ NaCl, 5 g l^{-N} yeast extract, and 10 g l^{-y} tryptone) and incubated at 37°C under shaking for 6 h. The cells were then washed and resuspended in MMG medium. Subsequently, the recombinant cassette (1 μg) was added to the GA1 cell suspension, adjusted to an OD_{600} of 0.01. The incubation was carried out at 37°C under shaking for 24 h. Colonies that had integrated the cassette through a double crossing over event were selected on LB plates supplemented with chloramphenicol (5 μg ml^{-1}), phleomycin (4 μg ml^{-1}) or kanamycin (5 μg ml^{-1}). The successful gene deletions were confirmed by PCR analysis using specific upstream and downstream primers (UpF and DwR) and by UPLC-MS to check the absence of production of the corresponding bioactive secondary metabolites. Mutants of *B. velezensis* were grown on LB medium supplemented with adapted antibiotics.

Trichoderma harzianum Rifai MUCL 29707 was obtained from the Mycothèque de l’Université catholique de Louvain (BCCM/MUCL). The strain was reactivated and periodically cultured on PDA. *Collimonas fungivorans* LMG 21973 was grown on TSA medium (Sigma-Aldrich, India) and obtain from the collection BCCM/LMG.

Solanum tuberosum L. var. Bintje was provided by the "Station de Haute Belgique" (Libramont, Belgium) as *in vitro* plants. The plants were micropropagated every 4 weeks in culture microboxes, sealed with breathing filters in the lid (ref: 0118/120 + OD118, $SacO_2$, Belgium). They were grown on sterilized (121°C for 15 min) Murashige and Skoog (MS) medium (Duchefa, Netherlands) supplemented with 10 g l^{-1} sucrose and solidified with 4.2 g l^{-1} phytagel (Sigma-Aldrich, St. Louis, USA). The microboxes were placed in a growth chamber (Snijders Scientific B.V., Netherlands), under a temperature of 20/18°C (day/night), a relative humidity (RH) of 75%, a photoperiod of 16 h day^{-1} and a photosynthetic photon flux (PPF) of 50 μmol s^{-1} m^{-2}.

Solanum lycopersicum cv Ailsa Craig and cv MoneyMakers seeds were obtained from EnGraineToi (Sussargues, France). Seeds were sterilized by immersion in 70% (v/v) ethanol for 1 min and 10% (v/v) sodium hypochlorite (NaOCl, 12%) for 4 min, then thoroughly rinsed in sterile water before their use in experiments.

The protective effect of tomato due to induced systemic resistance was performed using *Botrytis cinerea* MUCL 43839 as pathogen agent. The strain was obtained from BCCM/MUCL.

METHOD DETAILS

Set up of experimental *in-vitro* system

Bi-compartmented Petri plates (90 × 15 mm) were used to grow transformed carrot roots with the AM fungi as detailed in St-Arnaud et al.[24] In one compartment (the root compartment – RC), the root and AM fungus were associated on 25 ml MSR medium.[25] The MSR medium was solidified with 4.2 g l^{-1} Phytagel, while in the other compartment (the hyphal compartment - HC), only the extraradical mycelium of the fungus was allowed to grow. The fungus extended in the HC via a slope (from top to bottom of the plastic barrier separating the RC from the HC) made of 5 ml MSR medium, without sucrose and vitamins (MSR^{min}), gelified with 10 g l^{-1} agarose. Ten ml of the same solid medium were poured in the HC (HC^{solid}). Agarose with high-purity ,without added sugar, was used to prevent residual bacterial growth, which we observed on Phytagel and agar-solidified media. After circa 3 months of growth, the extraradical mycelium (ERM) network of *R. irregularis*, *R. clarus*, *R. aggregatus* and *R intraradices* extended profusely in the HC (thereafter $HC^{solid+Ri}$) (Figure S5). A control treatment consisting of non-mycorrhizal excised transformed carrot roots was included and roots were allowed to cross the partition wall separating RC from HC to grow for circa 3 months in the HC (thereafter $HC^{solid+Dc}$) (Figure S5). The system was further developed with the HC containing liquid MSR medium, with the exception of the slope.[15] Briefly, in the HC, 15 ml of liquid MSR^{min} medium diluted twice ($MSR^{min-½}$) was added (HC^{liquid}). After 3 months, a profuse ERM has developed in the HC ($HC^{liquid+Ri}$) (Figure S5). Bi-compartmented Petri plates were incubated in the dark at 27 °C.

Similarly, to the above, bi-compartmented Petri plates were used to grown *Solanum tuberosum* var Bintje plantlets. Twenty days old *in vitro S. tuberosum* plantlets were transferred in the Petri plates with their shoot protruding outside the plate via a small opening in the lid, plastered with sterile silicon grease to avoid contaminations, and the roots developing in the RC on 20 ml MSR^{min} medium. The roots crossed the partition wall and developed in the HC on the MSR^{min}medium gelified with 10 g l^{-1} of agarose ($HC^{solid+St}$)(Figure S5). Fresh medium was added weekly to keep medium at the top of the partition wall in the RC. The plants were kept for ~3 months in a growth chamber (Snijders Scientific B.V., Netherlands), under a temperature of 20/18°C (day/night), a RH of 75%, a photoperiod of 16 h day^{-1} under a PPF of 50 μmol s^{-1} m^{-2}.

In complement to the bi-compartmented Petri plates, a tri-compartmented *in vitro* culture setup was developed only for *R. irregularis* MUCL 41833. In this system, the roots were paired with the AM fungus in one compartment (referred to as the root compartment - RC). From this RC, the ERM extended into two adjacent compartments (referred to as the hyphal compartments - HC). The compartment containing the root culture was supplied with MSR, whereas the two hyphal compartments contained MSR without sucrose and vitamin (MSR^{min}) and were solidified with agarose (HC^{solid}). In these HCs, only the ERM of the fungus was allowed to grow ($HC^{solid+Ri}$), while the roots were confined to the RC (Figure 3G).

When necessary, roots that crossed the plastic barrier into the HC were either redirected back into the root compartment (RC) to prevent them from growing into the hyphal compartment.

Root and hyphae colonization by *B. velezensis in vitro*

After 4 weeks of growth, the ERM in the $HC^{solid+Ri}$ or transformed roots in the $HC^{Solid+Dc}$ treatments were inoculated with *B. velezensis* GFP-tagged and colonization of hyphae or roots was monitored by microscopy. To do so, the bacterial cells were precultured overnight in liquid root exudates mimicking exudates of *Solanaceae* (RE)[55] medium under shaking (180 rpm). The cells were then washed twice with physiological water (NaCl 0.9% w/v) and bacterial concentration was adjusted to 7.5×10^8 CFU ml^{-1}. A single *R. irregularis* hyphae or root of *D. carota* was inoculated with one drop of 1 μl of bacterial suspension. The colonization of GA1 GFP-tagged was monitored at regular intervals. Microscopic composite pictures were obtained by epifluorescence microscopy to determine the speed of bacterial colonization along hyphae or roots of *D. carota*. The speed of colonization was quantified by measuring the distance travelled by *B. velezensis* from the inoculation drop divided by the day post inoculation (dpi). The quantification was performed from the biological material of minimum 7 plates (biological replicates) at 3, 7 and 14 dpi.

Microscopy imaging was performed using a Nikon Ti2-E inverted microscope (Nikon, Japan) equipped with ×20/0.45 NA S Plan Fluor objective lenses (Nikon, Switzerland) and a Nikon DS-Qi2 monochrome microscope camera. Images and videos taken in the bright field channel were acquired using a Ti2 Illuminator-DIA and an exposure time of 20 ms. *B.velezensis* GFP-tagged was visualized by conventional epifluorescence microscopy. A lumencor sola illuminator (Lumencor, USA) was used as source of excitation with an exposure time of 500 ms and the GFP-B HC Bright-Line Basic Filter was used.

Velocity of cytoplasmic flow

The velocity of cytoplasmic flow inside hyphae of *R. irregularis*, colonized or not by *B. velezensis*, was measured at 3, 7 and 14 dpi of the bacterium or for the control, by capturing videos in the bright field channel as described in section "Root and hyphae colonization by *B. velezensis in vitro*". The inoculation of hyphae by *B. velezensis* or GA1 mutants was also performed as previously described in section "Root and hyphae colonization by *B. velezensis in vitro*". The control treatment involved treating non-colonized hyphae with 1 μl of physiological water. The velocity of cytoplasmic flow colonized by *B. velezensis* mutants was evaluated only at 7 dpi.

The cytoplasmic flow velocity of *R. irregularis* was also quantified in the presence of pure surfactin. Hyphae of *R. irregularis* were inoculated with 1 μl of pure surfactin solubilized by sonication in PBS at 2 μM, 20 μM or 50 μM concentration. A control treatment with only 1 μl PBS was included.

To investigate the impact of surfactin on the distal regions of the *R. irregularis* ERM network away from direct contact with the lipopeptide, a second experiment was conducted using a three-compartment Petri plate system. One of the two hyphal compartments was treated (the Treated compartment), either with a pure surfactin solution at 2 μM ($HC^{solid+Ri+srf}$) or PBS ($HC^{solid+Ri+PBS}$). The second hyphal compartment remained untreated but was labelled according to its proximity to the treated compartment, either with surfactin ($HC^{solid+Ri-srf}$) or with PBS ($HC^{solid+Ri-PBS}$). These three compartments were separated by plastic barriers, preventing direct physical connections between them. However, the fungal ERM network itself remained continuous and interconnected through the root compartment. The velocity of cytoplasmic flow in *R. irregularis* was quantified in each one of the 4 HC.

For all experiments, measurements were conducted on a minimum of 4 plates (biological replicates) in which minimum 4 video were taken (technical replicate) following the treatment. We processed the data by Manual tracking plug-in inside the Tracking tool in the Plug-in menu in Fiji[48,97,98] (Videos S4 and S5). Thus, using the Manual tracking minimum 8 particles were tracked in each video. For each graph regarding the velocity, each point represents the average of four measurements in each direction, which can be considered technical replicates. Velocity was calculated for each tracked object during minimum 10 frames with the video taken with a speed of 10 fps during 10 seconds (100 frames/video), depending on how long the object could be followed. At four mycelial locations, clear evidence of bi-directional transport was detected. Consequently, we measured the velocity of cellular contents similar to PIV analysis, as illustrated in Videos S4 and S5. The isolation and tracking of cellular contents were performed from DIC images.

Succinate dehydrogenase (SDH) activity in hyphae

Histochemical staining was performed to quantify the succinate dehydrogenase (SDH) activity according to the adapted procedures of Schaffer and Peterson.[46] The SDH activity of *R. irregularis* hyphae was assessed 7 and 14 dpi with *B. velezensis* ($HC^{Solid+Ri}$) and compared to hyphae non-inoculated with the bacterium (1 μl of physiological water - 0.9 % (w/v)) and to hyphae killed with formaldehyde (2 % (v/v)).[101] The inoculation of hyphae by *B. velezensis* was performed as previously described in section "Root and hyphae colonization by *B. velezensis in vitro*". The AM fungal hyphae developing on the surface of the MSR^{min} medium in the $HC^{Solid+Ri}$ treatment were harvested with a needle. Briefly, hyphae were immersed in a solution containing 0.2 M Tris-HCl pH 7.4, 1 M sodium succinate hexa-hydrate, 1 mg ml^{-1} nitro blue tetrazolium (NBT) and 5 mM $MgCl_2$. The SDH, present in viable fungal hyphae, reacts with NBT and is reduced to a dark blue-violet formazan compound. The hyphae were washed with 1 ml of physiological water (0.9 % (w/v)). A second staining, was performed with fuchsin acid (0.1% (v/v)) to obtain better contrast. The samples were then cleaned in a solution of lactoglycerol. Pictures of the stained hyphae were taken in the brightfield channel by stereomicroscopy. A Nikon SMZ1270 stereomicroscope (Nikon, Japan) equipped with a Nikon DS-Qi2 monochrome microscope camera and a DS-F 2.5 F-mount Adapter 2.5× was used. The stereomicroscope was used with an ED Plan 2×/WF objective (Nikon, Switzerland) and an OCC illuminator allowing the image capture in the brightfield channel at an exposure time of 40 ms. The images were processed using Fiji[97] by measuring, by threshold settings, the total surface of the hyphae and the surface corresponding to potential SDH activity. The SDH activity was calculated by the following formula: $\text{relative dark area}\ (\%) = \frac{\text{dark area}}{\text{total area}} \times 100$. The quantification was performed from the biological material of minimum 3 plates (biological replicates) where minimum 1 hyphae has been harvested by plate (technical replicate).

Impacts of BSMs on AM fungal hyphae

The impact of lipopeptides of *B. velezensis* (i.e. surfactin, iturin and fengycin) was tested on hyphae integrity. The potential permeabilization of the AM fungus membrane was quantified using fluorescent intercalating propidium iodide (PI) that is not internalized by healthy cells. Four hyphae per Petri plate developing at the surface of the $HC^{Solid+Ri}$ medium were exposed to one drop of 1 μl of 2 μM, 20 μM or 50 μM of iturin, surfactin or fengycin and incubated at room temperature for 30 min. Ten μl of PI solution at 50 μg ml^{-1} was then applied on each hyphae for 15 min at room temperature in the dark. The stained hyphae were visualized by fluorescence microscopy (Nikon Ti2-E) with appropriate filters (TexasRed HC BrightLine Basic Filter). A PBS solution (Control) and a positive control in which hyphae were treated with 1% Triton X-100 with 2% formaldehyde (Killed) were considered. PI fluorescence was quantified using NIS-Element AR software (Nikon, Japan). The membrane permeabilization was assessed by threshold settings to obtain the region of interest (ROI) within the images taken in the bright field channel corresponding to hyphae area. Within this ROI, the mean of red intensity (MeanRed), equivalent at the arithmetic mean of pixel intensities, was quantified in the images taken in the red channel. The experiment was performed in 3 biological replicates (3 Petri plates) per treatment.

Bacterial CFU counting *in vitro*

The colonization density of *B. velezensis* GA1 GFP-tagged on *D. carota* transformed roots ($HC^{solid+Dc}$), *R. irregularis* hyphae ($HC^{solid+Ri}$) and *S. tuberosum* roots ($HC^{solid+St}$) was quantified. Bacterial inoculation was performed as previously described in the section "Root and hyphae colonization by *B. velezensis in vitro* ".

The colonization density of roots and hyphae as well as spores produced by the bacteria were evaluated at 3, 7 and 14 dpi of *B. velezensis* for AM fungal hyphae and roots of *D. carota*, while for *S. tuberosum* roots, it was performed at 14 dpi. Colonization was evaluated on 2 cm of roots or AM fungal hyphae proximal of the inoculation drop area. Bacterial cells were detached from roots and hyphae by vortexing them for 5 min in a solution of physiological water supplemented with 0.1% (vol/vol) Tween 80 and 6 glass beads. To evaluate the number of bacterial spores, half of each solution was incubated at 80°C during 25 min to kill all vegetative cells. The colonies were counted by performing serial dilutions plated onto LB medium solidified with 14 g l^{-1} of agar. Plates were incubated for 12 h at 30°C. The quantification was performed from the biological material of minimum 4 replicates (i.e. plates) divided into 3 sample for each treatment. The results were expressed following the available area provided by each host depending of the sampling length (2cm) and of the average diameter of each host (Figure S6). This approach allows to evaluate bacterial colonization for the same length of sample and according to the colonizable surface area for each host.

Likewise, the colonization density of *B. velezensis* GA1 GFP-tagged on *R. clarus*, *R. aggregatus*, and *R. intraradices* was evaluated also at 7 dpi. The colonization of the different mutants (*ΔituA-ΔfenA, ΔsrfaA, ΔsrfaA-fenA, ΔsrfaA-ΔituA, ΔsrfaA-ΔituA-ΔfenA and Δsfp*) were evaluated only on *R. irregularis* MUCL 41833.

B. velezensis biofilm formation along AM fungal hyphae of *R. irregularis*

To evaluated the formation of biofilm by *B.velezensis* on AM fungal hyphae of *R. irregularis*, we assessed the colonization density of *B. velezensis* GA1-GFP tagged and the knockout mutants *ΔepsA-O* and *ΔtasA*, as previously described.

The growth of these mutants was tested to confirm that the mutations did not impact growth. To further validate this, we monitored the continuous growth kinetics of *B. velezensis* WT and knockout mutants in RE[55] medium using 96-well microplates (Figure S2C).

First, a pre-culture of *B. velezensis* and of mutants were prepared at 30°C in liquid RE medium under shaking (180 rpm) overnight. The pre-cultures were washed twice with physiological water (0.9% w/v NaCl). The bacterial suspensions were then adjusted to an OD600 of 0.05 in the 96-well microplate, with a final volume of 200 μl per well. The growth kinetics of B. velezensis WT and mutants (OD600) were monitored every hour for 36 h using a Tecan Spark automatic plate reader (Tecan Group Ltd, Männedorf, Switzerland) under continuous shaking at 30°C (Figure S2B).

B. velezensis metabolite production along AM fungal hyphae

Metabolites produced by *B. velezensis* GA1 GFP-tagged developing in contact with hyphae were extracted and analyzed by LC-MS. As previously described in the section "Root and hyphae colonization by *B. velezensis in vitro* ", *B. velezensis* was inoculated on the surface of hyphae in the HC ($HC^{Solid+Ri}$). After 9 days, a plug of agarose gel (0.5 cm × 2.5 cm) containing *R. irregularis* hyphae and the bacterium was sampled. BSMs were extracted via the application of 400 μl of acetonitrile (ACN) (75 % vol/vol) during 30 min. Then, the extract was filtered with hydrophilic PTFE syringe filters ROCC S.A. (0.22 μm pore size) before UPLC-qTOF MS analysis.

Briefly, the extracts were analyzed using a Agilent 1290 Infinity II apparatus coupled with a diode array detector and mass detector (Jet Stream ESI-Q-TOF 6530) with the parameters: capillary voltage: 3.5 kV; nebulizer pressure: 35 psi; drying gas: 8 l min^{-1}; drying gas temperature: 300°C; flow rate of sheath gas: 11 l min^{-1} sheath gas temperature: 350 °C; fragmentor voltage: 175 V; skimmer voltage: 65 V; octopole RF: 750 V. Accurate mass spectra were recorded in positive mode in the range of m/z =100–1700. Metabolites (injection volume, 10 μl) were separated on C18 Acquity UPLC BEH column (2.1 × 50 mm × 1.7 μm; Waters, milford, MA, USA) and elution was performed as follows: acetonitrile and distilled water as solvents (both supplemented with 0.1% (vol/vol) formic acid), a flow rate of 0.6 ml min^{-i} and gradient over 20 min (programe: initial 10% (vol/vol) acetonitrile during 1 min before increase to 100% (vol/vol) over 20 min, held at 100% (vol/vol) for 3.5 min).

The identified BSMs were quantified by their peak area values using MassHunter v10.0 workstation. The CLiPs were quantified based on their retention times and accurate masses compared with pure molecule standards.

The relative proportion of the detected CLiPs was then calculated by following formula:

$$\text{Relative lipopeptide proportion}\ (\%) = \frac{\text{Lipopeptide area}\ (\text{One family})}{\text{Lipopeptides total area}\ (\text{All families})} \times 100$$

B. velezensis metabolite production on *R. irregularis* exudates

The metabolite production of *B. velezensis* grown on *R. irregularis* exudates was analysed by LC-MS. To observe the effect of *R. irregularis* exudates on the BSMs production of GA1, the ERM of *R. irregularis* was cultivated on $MSR^{min-1/2}$ liquid medium ($HC^{Liquid+Ri}$). After 4 weeks of *R. irregularis* growth, the liquid medium was collected and hyphal exudates of 5 different plates were grouped. At least 15 hyphal exudate solutions from 15 individual plates were grouped in 3 distinct solutions. The exudates harvested were freeze-dried (Freeze-dryer Alpha 3-4 LSCbasic brand Christ), resuspended and concentrated 5 times with a solution containing MOPS buffer (10.5 g l^{-1}) and NH_4SO_4 (1 g l^{-1}). The exudates concentrated 5 times were sterilized with CA syringe filters ROCC S.A. (0.22 μm pore size).

Then, the continuous growth kinetics of *B. velezensis* in AM fungal exudates was followed in 96 wells microplates. First, a pre-culture of *B. velezensis* was done at 30°C in liquid RE medium[55] under shaking (180 rpm) overnight. The preculture was washed twice with physiological water (Na Cl 0.9 % w/v). The bacterial suspension was adjusted to obtain an OD_{600} of 0.05 into the 96 wells microplate in a final volume of 200 μl per well. The growth of *B. velezensis* was measured in 5 times concentrated exudates of *R. irregularis*. The growth kinetics of *B. velezensis* (OD_{600}) was followed every hour during 36 h on a Tecan Spark automatic plate reader (Tecan Group Ltd, Männedorf, Switzerland) under continuous shaking at 30°C. To study the effect of hyphal exudates on the GA1 metabolome, 3 wells of each condition were grouped, filtered (0.22 μm) and then analyzed by LC-MS as previously described in the section "*B. velezensis* metabolite production along AM fungal hyphae". At least 3 distinct concentrated hyphal solutions (biological replicates) were inoculated with minimum 2 distinct *B. velezensis* precultures.

B. velezensis metabolite production on carbohydrate compounds present in *R. irregularis* exudates

The influence of carbohydrate compounds in the hyphal exudates of the AM fungus, often reported in the literature, was evaluated on BSMs production of GA1 WT. The carbon sources of AM fungus exudates (10 mM of fructose, glucose, inositol, citric acid, 5 mM trehalose and 15 mM succinic acid) were solubilized in M9 minimal salts medium (KH_2PO_4 3 g l^{-1}; NaCl 0.5 g l^{-1}; Na_2HPO_4 6.78 g l^{-1}; NH_4Cl 1 g l^{-1}) supplemented with 2 mM $MgSO_4$, 0.1 mM $CaCl_2$, 10 μM $FeSO_4$ and buffered at pH 6.8 with MOPS (10.5 g l^{-1}) forming the so-called Arbuscular Mycorrhizal Fungi Exudate Mimicking Medium (AMF-EMM). The metabolite production of GA1 was followed as previously described in the section "*B. velezensis* metabolite production along AM fungal hyphae". The experiment was performed in 3 biological replicates (3 precultures of *B. velezensis*) with minimum 4 technical replicates for each biological replicate.

B. velezensis antimicrobial activity assays on hyphal exudates

Antimicrobial activity of GA1 wild type (WT) or GA1 mutant cell-free supernatants (CFS) produced on hyphal exudates of *R. irregularis* was assessed against *Trichoderma harzianum* Rifai MUCL 29707 and *Collimonas fungivorans* LMG 21973. To do so, GA1 WT and its mutants (Table S1) were cultivated on exudates of *R. irregularis* as describe in section "B. *velezensis* metabolite production on *R. irregularis* exudates". The CFS of these cultures were obtained by centrifugation of the bacterial culture at 10000 rpm and sterilization with a PTFE syringe filters ROCC S.A. (0.22 μm pore size).

To observe the effects of GA1 WT or GA1 mutant CFS on the growth of *T. harzianum*, fungal spores were harvested from 10 days old PDA cultures and suspended at a concentration of 2×10^5 CFU mL^{-1} with physiological water supplemented with 0.1% (vol/vol) Tween 80. Ten μl of fungal spores were then resuspended into a 96 wells microplates with final volume of 200 μl / wells adjusted with PDB medium supplemented with 20% (vol/vol) of GA1 WT or GA1 mutant CFS. The control was complemented with physiological water supplemented with 0.1% (vol/vol) Tween 80. The growth kinetics of *T. harzianum* (OD_{600}) was followed every hour during 36 h with a Tecan Spark automatic plate reader (Tecan Group Ltd, Männedorf, Switzerland) under continuous shaking at 26°C. Three independent assays, each involving minimum 4 technical replicates, were performed.

To evaluate the impact of CFS on the growth of *C. fungivorans*, a bacterial suspension of this bacterium was prepared by centrifuging the overnight preculture, washing the cells twice, and resuspending them in physiological water. The bacterial suspension was adjusted to obtain an OD_{600} of 0.05 into the 96 wells microplate, with a final volume of 200 μl / well-adjusted with TSA medium (Sigma-Aldrich, India) supplemented with 20% (vol/vol) of GA1 WT or GA1 mutant CFS. The control was complemented with physiological water. The growth kinetics of *C. fungivorans* (OD_{600}) was followed every hour during 24 h on a Tecan Spark automatic plate reader (Tecan Group Ltd, Männedorf, Switzerland) with continuous shaking at 26°C. Three independent assays each involving 6 technical replicates were performed.

Translocation of surfactin via the AM fungal network

The transport of surfactin across the fungal network was assessed using the tri-compartment Petri plate system, as described in section "Velocity of Cytoplasmic Flow". To investigate the effectiveness of AM fungal hyphae in transporting surfactin, 10 ml of a 20 μM surfactin solution we applied to one of the hyphal compartments, covering the entire compartment (referred to as $HC^{solid+Ri+srf}$). To determine whether surfactin was translocated through the ERM, a control experiment was conducted in which the *R. irregularis* ERH network was cut before the surfactin application along the entire length of the compartment and on 0.5 cm of width, creating an air gap in the non-inoculated compartment. Subsequently, we collected the medium from the treated and the non-treated hyphal compartments. After extraction, the surfactin contents in each hyphal compartment were determined by LC-QTOF MS analysis of the surfactin contents of each hyphal compartment, following the procedures outlined in section "*B. velezensis* Metabolite Production Along AM Fungal Hyphae". This experiment was carried out in 3 biological replicates, with 3 plates for each condition.

Experimental design of greenhouse trial for *B. velezensis* common mycorrhizal network colonization

Two 500 ml pots, referred as Pot 1 and Pot 2, were connected by a 4.5 cm diameter pipe made of HDPE (High-density polyethylene) (Figure 2D). Both ends of the tube were sealed with a nylon mesh of 50 μm porosity to prevent the passage of plant roots from one pot to the other. Each pot contained a sterile mixture of sand/vermiculite/loam (45%:45%:10%, v/v/v). One 20 day-old *S. tuberosum* plantlet grown *in vitro* was planted in each pot. Prior to the planting, 8 plants in pot 1 were inoculated with 10 g of *R. irregularis* inoculum (+ *R.i.*). The inoculum was obtained by associating isolated spores from an *in vitro* culture of the AM fungus with maize plants (*Zea mays* L. cultivar ES Ballade) grown in sterilized lava stone (DCM, Belgium) for 4 months. The total root colonization by *R. irregularis* MUCL41833 reached 88%. The roots and the rhizospheric substrate attached to these plants were homogenized

and used as *R. irregularis* inoculum.[35,102] Additionally, 8 other plants of pots 1 were inoculated with 10 g of autoclaved (121°C for 15 min) *R. irregularis* inoculum (- *R.i.*). The plants were grown in greenhouse at 25 °C with a RH of 75% and a 16/8 h (day/night) photoperiod under a PPF of 120 mmol s^{-1} m^{-2}. The plants were watered once a week with distilled water and fertilized once a week with Hoagland nutrient solution impoverished in phosphorus (Hoagland^{-P}).[102] After 3 months of growth, each plant in pot 1 was inoculated with 50 ml of a bacterial suspension of *B. velezensis* GA1 GFP-tagged. This suspension was prepared by centrifuging an overnight culture (RE medium, 26°C), washing the cells twice, and resuspending them in Hoagland^{-P} to a cellular density of 5 × 10^8 CFU ml^{-1}. The 16 uninoculated plants in pots 2 were treated with 50 ml of Hoagland^{-P} solution without any microorganisms. The colonization of *R. irregularis* and *B. velezensis* on the roots of plants in pots 1 and in pots 2 were quantified 20 days after the inoculation of *B. velezensis* as described in section "Mycorrhizal root colonization under greenhouse trials" and "Bacterial root colonization under greenhouse trials".

Effect of *B. velezensis* colonization on AM fungal population under greenhouse trial

The potential influence of the bacterial colonization on the *R. irregularis* population was evaluated under greenhouse conditions. Briefly, 16 pots were inoculated with 5 g of *R. irregularis* inoculum as previously described in section "Experimental design of greenhouse trial for *B. velezensis* common mycorrhizal network colonization". At the same time, a sterilized seed of tomato cv Money Makers was sown in each pot. The plants were grown in greenhouse at 25 °C with a RH of 75% and 16/8 h (day/night) photoperiod under a PPF of 120 mmol s^{-1} m^{-2}. The plants were watered once a week with distilled water and fertilized once a week with Hoagland^{-P}. After 5 months, to observe the effect of *B. velezensis* on *R. irregularis* population, 8 pots containing plants were watered with 50 ml of a bacterial solution of GA1 GFP-tagged as previously described (*B.v.*+ *R.i.*). The remaining pots were watered with 50 ml of Hoagland^{-P} solution without *B. velezensis* (*R.i.*). The colonization of *R. irregularis* and *B. velezensis* on the roots of plants for each condition was quantified before the bacterial inoculation and 7 days after the inoculation of *B. velezensis* as described in section "Mycorrhizal root colonization under greenhouse trials" and "Bacterial root colonization under greenhouse trials".

ISR induction in tomato plants under greenhouse condition

Sterilized Ailsa Craig seeds were transferred to 1 l pots containing a sterile substrate of sand/vermiculite/loam (45%:45%:10%,v/v/v). For each treatment, 16 pots were used. Each one of the 16 pots was supplemented with 5 g of *R. irregularis* inoculum containing AM fungal-colonized roots and spores (*R.i.*) prepared as previously described in section "Experimental design of greenhouse trial for *B. velezensis* common mycorrhizal networkcolonization". The inoculation of tomato plants with *R. irregularis* was done by mixing the substrate with the AM fungal inoculum prior to sowing.

Likewise, 16 plants were watered with 10 ml of a bacterial solution (*B.v.*) as described in section "Experimental design of greenhouse trial for *B. velezensis* common mycorrhizal network colonization". Additionally, 16 pots were co-inoculated with both the bacteria and the AM fungus (*R.i.* +*B.v.*) as described for the treatment with one microorganism. A second bacterial application was performed after 12 weeks of plant growth by inoculating the plants with 10 ml of a bacterial solution at the same concentration. A control group composed of 16 non-inoculated plants and supplemented with the same amount (5 g) of AM fungal sterilized (121°C for 15 min) inoculum substrate was treated with Hoagland^{-P} solution without the bacterial solution.

The plants were grown in the greenhouse at 25 °C with a RH of 75% and 16/8 h (day/night) photoperiod under a PPF of 120 mmol s^{-1} m^{-2} for 3 months. They were watered once a week with non-sterilized distilled water and were also fertilized once a week with Hoagland^{-P}. The pots were arranged in a fully randomized design.

At week 13, the plants were infected with *B. cinerea* MUCL 43839. Prior to infection, the size of the plants was measured to assess the impact of the combined treatment on plant growth compared to the control plants (n = 16/treatment). *B. cinerea* was routinely cultured on potato dextrose agar at 26°C from a spore suspension stored at -80°C. *B. cinerea* spores were collected from 15 days-old cultures in physiological water containing 0.01% Tween 20. The spore suspension was then filtered (Whatman, Grade1), quantified and adjusted to a concentration of 5 × 10^6 spores ml^{-1}. Infection was performed by applying 10 μl droplets of the spore suspension onto 5 leaflets of the third, fifth and sixth leaves of each plant (15 infected leaflets/plant). The disease severity of *B. cinerea* on tomato leaves was assessed 14 dpi by measuring the lesion area using ImageJ (n = 8/treatment).

The colonization of *R. irregularis* and *B. velezensis* in the combined treatment (*B.v.* + *R.i.*) was quantified at 14 and 21 dpi after the second GA1 treatment (n = 8/times) as described below.

Microbial root colonization under greenhouse trials

To determine *B. velezensis* colonization, bacterial cells were detached from samples of 1 g of roots including attached rhizospheric substrate samples by vortexing for 5 min in a solution of physiological water supplemented with 0.1% (vol/vol) Tween 80 and 6 glass beads. The colonies were counted by performing serial dilutions plated onto LB medium supplemented with chloramphenicol 5 μg l^{-1}. Plates were incubated for 12 h at 30 °C, and the results were expressed as the number of CFU of *B.v.* g^{-1} of sample.

To determine the mycorrhizal status of the plants, roots with attached rhizospheric substrate were sampled to quantify the presence of *R. irregularis* by qPCR. Frozen roots were crushed in liquid nitrogen, and DNA was extracted from a 500 mg crushed root sample using GenEluteTM Soil DNA Isolation kit (Sigma-Aldrich, Canada) with slight modifications. Prior to extraction, a lysis step was performed using DNAzol™ Reagent under shaking and homogenization with FastPrep-24™ (MP Biomedical's, Germany). The concentration and purity of the extracted DNA were assessed with the UV-vis spectrophotometer NanoDrop 2000 (Thermo scientific). qPCR was performed in an ABI StepOne™ qPCR apparatus (Applied Biosystems) using the kit Luna® Universal qPCR Master

Mix Kit (New England Biolabs, Ipswich, MA, United States). PCRs were conducted in a total volume of 20 μl containing 10 μl of Luna Universal qPCR Mix, 0.5 μl of each primer (10 μM) and 5 μl of DNA. The qPCR protocol consisted of an initial denaturation step at 95°C (1 min), followed by 40 cycles of denaturation (95°C, 15 s) and extension (60°C, 30 s). Melting curves were also generated from 65 to 95°C with an increase rate of 0.5°C/ 5 s to evaluate the specificity of the amplified products. The strain-specific primer pair for *R. irregularis* MUCL41833 targeting the mtLSU region was used: forward 5'-AAGTCCTCTAGGTCGTAGCA-3' and reverse 5'-ACAGGTATTTATCAAATCCTTCCC-3'. The resulting concentrations were expressed as mg of R.i. g^{-1} of sample. The quantification of *R. irregularis* was performed based on the standard calibration curves (Figure S7). To prepare standards for the qPCR experiment, DNA extracted from *R. irregularis* spores and mycelium grown *in vitro* were used. Spores/mycelium of 3 months old cultures were extracted from HC following solubilization of the phytagel with citrate-buffer. Five mg of spores/mycelium were quantified and lysed with DNAzoleTM. A serial 4-fold dilutions of the lysed extraction with DNAzole (5×10^{-1}–10^{-1} mg μl^{-1}) was performed prior to the DNA extraction, following the same procedure described above for roots.

Quantification and statistical analysis

Data were processed using GraphPad Prism 9.2.0 software to perform statistical analysis. The impact of factors (experiments, treatments, biological materials and dpi) on variability were considered in the statistical general analyses to analyse repeated measure experiments. Differences were considered statistically significant at $p < 0.05$.